Major and trace element geochemistry of plutonic rocks from Francistown, NE Botswana: evidence for a Neoarchaean continental active margin in the Zimbabwe craton

A.B. Kampunzu[a,*], A.R. Tombale[b], M. Zhai[a], Z. Bagai[a], T. Majaule[c], M.P. Modisi[a]

[a] *Department of Geology, University of Botswana, Private Bag 0022, Gaborone, Botswana*
[b] *Ministry of Mineral, Energy and Water Affairs, Private Bag 0018, Gaborone, Botswana*
[c] *Department of Geological Survey, Private Bag 14, Lobatse, Botswana*

Abstract

The Neoarchaean Tati granite–greenstone terrane occurs within the southwestern part of the Zimbabwe craton in NE Botswana. It comprises 10 intrusive bodies forming part of three distinct plutonic suites: (1) an earlier TTG suite dominated by tonalites, trondhjemites, Na-granites distributed into high-Al (Group 1) and low-Al (Group 2) TTG sub-suite rocks; (2) a Sanukitoid suite including gabbros and Mg-diorites; and (3) a younger high-K granite suite displaying I-type, calc-alkaline affinities.

The Group 1 TTG sub-suite rocks are marked by high Sr/Y values and strongly fractionated chondrite-normalized rare earth element (REE) patterns, with no Eu anomaly. The Group 2 TTG sub-suite displays higher LREE contents, negative Eu anomaly and small to no fractionation of HREE. The primordial mantle-normalized patterns of the Francistown TTGs are marked by negative Nb–Ti anomalies. The geochemical characteristics of the TTG rocks are consistent with features of silicate melts from partial melting of flat subducting slabs for the Group 1 sub-suite and partial melting of arc mafic magmas underplated in the lower crust for the Group 2 sub-suite. The gabbros and high-Mg diorites of the Sanukitoid suite are marked by Mg#>0.5, high Al_2O_3 (>>16%), low TiO_2 (< 0.6%) and variable enrichment of HFSE and LILE. Their chondrite-normalized REE patterns are flat in gabbros and mildly to substantially fractionated in high-Mg diorites, with minor negative or positive Eu anomalies. The primordial mantle-normalized diagrams display negative Nb–Ti (and Zr in gabbros) anomalies. Variable but high Sr/Y, Sr/Ce, La/Nb, Th/Ta and Cs/La and low Ce/Pb ratios mark the Sanukitoid suite rocks. These geochemical features are consistent with melting of a sub-arc heterogeneously metasomatised mantle wedge source predominantly enriched by earlier TTG melts and fluids from dehydration of a subducting slab. Melting of the mantle wedge is consistent with a steeper subduction system. The late to post-kinematic high-K granite suite includes I-type calc-alkaline rocks generated through crustal partial melting of earlier TTG material. The Neoarchaean tectonic evolution of the Zimbabwe craton is shown to mark a broad continental magmatic arc (and related accretionary thrusts and sedimentary basins) linked to a subduction zone, which operated within the Limpopo–Shashe belt at ~ 2.8–2.65 Ga. The detachment of the subducting slab led to the uprise of a hotter mantle section as the source of heat inducing crustal partial melting of juvenile TTG material to produce the high-K granite suite.

Keywords: Petrogenesis; Continental arc; TTG; Sanukitoids; High-K granites; Zimbabwe craton; Botswana

* Corresponding author.
E-mail address: kampunzu@mopipi.ub.bw (A.B. Kampunzu).

1. Introduction

The Zimbabwe craton has a complicated tectonic and magmatic history, which is the subject of much controversy. The oldest crustal rocks preserved in this craton (Fig. 1) are ~ 3.57–3.45 Ga in age and occur within the Tokwe segment (Wilson et al., 1995; Horstwood et al., 1999; Dodson et al., 2001), although Re–Os isotopic analyses of chromites from Archaean ultramafic rocks indicated that the Zimbabwean subcontinental lithospheric mantle began to be separated from the asthenospheric mantle before 3.8 Ga (Nägler et al., 1997). Kusky and Kidd (1992) suggested that the Belingwe greenstone belt is a remnant of an oceanic plateau allochthon. However, the existence of an old (Mesoarchaean) continental crust allowed several workers to model the Neoarchaean evolution of the Zimbabwe craton in terms of continental rifting above mantle plumes (e.g. Bickle et al., 1994; Jelsma et al., 1996; Hunter et al., 1998). Blenkinsop et al. (1993) and Bickle et al. (1994) contend that the Belingwe greenstone belt was emplaced in an ensialic setting. The 2.75–2.65 Ga igneous rocks from the Zimbabwe craton are tonalite–trondhjemite–granite and tholeiitic and calc-alkaline volcanic suites emplaced in arc and back-arc settings (e.g. Condie and Harrison, 1976; Jelsma et al., 2001). The greenstone belts (e.g. Tati) aligned along the southern part of the Zimbabwe craton (Fig. 1) and the Matsitama greenstone belt in northeast Botswana were taken for allochtonous sheets along the suture of an ocean closed at ca. 2.7 Ga (Kusky, 1998). The Matsitama greenstone belt is part of the Limpopo–Shashe orogenic belt (Ranganai et al., 2002) and this raises the question of the geotectonic relations between the evolution of the Zimbabwe craton and the Limpopo belt. A number of workers (Coward et al., 1976; McCourt and Wilson, 1992) indicated that the Zimbabwe craton was affected by shortening in response to Neoarchaean northerly thrusting of the Northern Marginal Zone (NMZ) of the Limpopo belt. The shear zones in the Zimbabwe craton are inferred to originate during the 2.6 Ga collision of the craton with the central zone of the Limpopo belt (Treloar et al., 1992; Rollinson, 1993; Treloar and Blenkinsop, 1995), although there is no agreement on this interpretation. Structural studies showed that several Neoarchaean greenstone belts of the Zimbabwe craton were affected by accretionary layer-parallel shear zones between ~ 2.7 and 2.6 Ga (Kusky and Kidd, 1992; Jelsma and Dirks, 2000). Dirks et al. (2002) reported an early episode of thin-skinned thrusting and a later steep west-directed thrusting and interpret these structures as indicating progressive accretion and crustal thickening marking a low-angle subduction or underplating. Steep geothermal gradients (~ 50 °C/km) characterise this tectonic crustal thickening (e.g. Jelsma and Dirks, 2000).

During the last decade, published geotectonic interpretations of the Zimbabwe craton focused on geochronological and structural data, with little emphasis on the geochemistry of igneous rocks (e.g. Condie and Harrison, 1976; Luais and Hawkesworth, 1994; Majaule et al., 1997; Jelsma et al., 2001). Geochemical studies of Archaean igneous rocks show a diversity of composition that matches that documented in modern igneous provinces emplaced in various tectonic settings (e.g. Dostal and Mueller, 1992; Hollings et al., 1999). Some workers (e.g. Hamilton, 1998) claim that Archaean granite–greenstone terranes mark igneous and tectonic processes different from Proterozoic and Phanerozoic plate tectonics. However, most igneous rock types recorded in Archaean terranes are known in Phanerozoic igneous provinces (e.g. Drummond and Defant, 1990; Martin, 1993) and therefore these modern analogues can be used for petrogenetic and geotectonic reconstruction of Archaean terranes.

The objectives of this paper are: (1) to present new chemical data of Neoarchaean plutonic rocks from the Zimbabwe craton exposed in the Tati granite–greenstone terrane in northeast Botswana; (2) to discuss the petrogenesis of the plutonic rocks and the tectonic setting during their emplacement; (3) to re-evaluate the relationship between the Zimbabwe craton and the Limpopo–Shashe belt during the emplacement of the Francistown granitoids and coeval igneous rocks in the Zimbabwe craton. The data in this paper are important for the understanding of Archaean accretionary processes in southern Africa and the formation, growth and preservation of the Archaean crust in the Zimbabwe craton.

2. Geological setting

The Zimbabwe craton is composed of granite–greenstone terranes emplaced between ca. 3.5 and 2.5

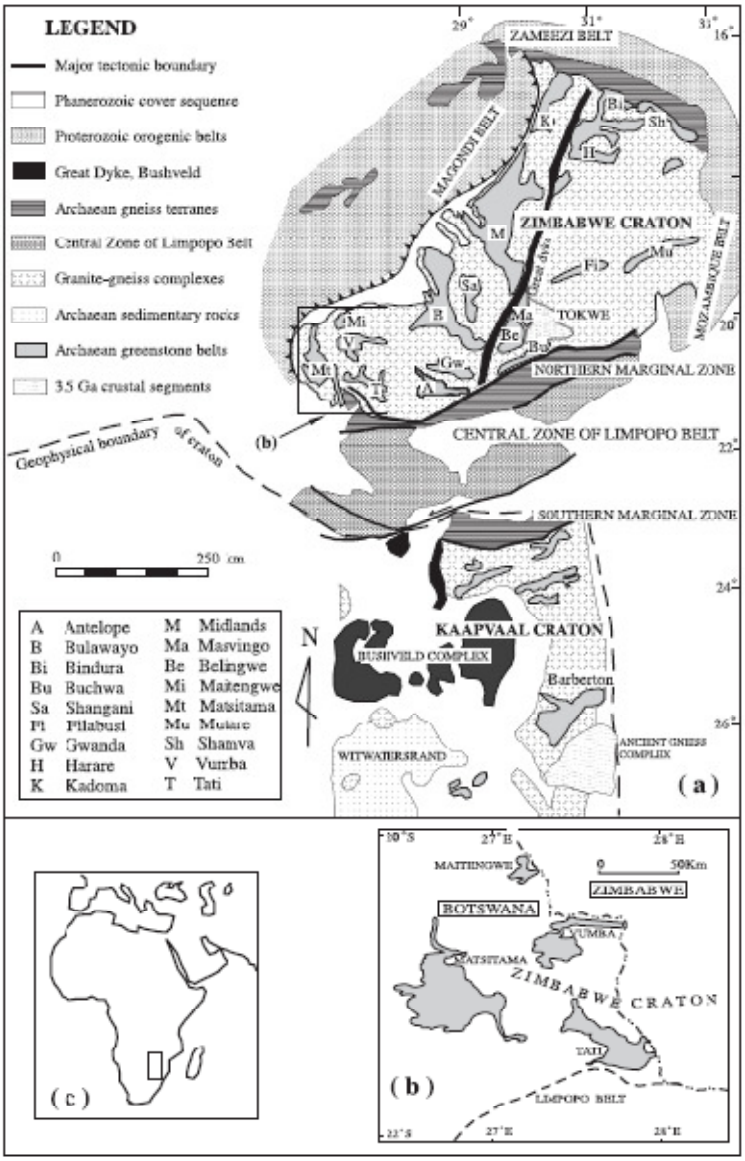

Fig. 1. (a) Map showing the main geological units of southern Africa cratons and adjacent Proterozoic belts (Bagai et al., 2002 and references therein). The rectangle locates the map of (b). (b) Distribution of the four main granite–greenstone terranes of the Zimbabwe craton in NE Botswana (slightly modified from Key et al., 1976). (c) Location of the southern Africa cratons in Africa.

Ga (Blenkinsop et al., 1997 and references therein). The southwestern margin of this craton extends into northeastern Botswana (Key et al., 1976) where four granite–greenstone terranes (Tati, Vumba, Maitengwe and Matsitama; Fig. 1) occur. The Matsitama granite–greenstone complex is dominated by shallow water clastic and chemical sedimentary rocks and minor mafic–ultramafic rocks (Aldiss, 1991; Majaule et al., 1997). Gravity data show that this granite–greenstone terrane is located within the Limpopo–Shashe belt (Ranganai et al., 2002) and the crustal thickness beneath the Matsitama area is ~ 50–55 km (Nguuri et al., 2001), in contrast to the cratonic areas where the crust is thinner (~ 35–37 km). U–Pb single zircon dating showed that the Matsitama granitoids were emplaced between 2710 ± 19 and 2646 ± 3 Ma (Majaule and Davis, 1998). These granitoids are time-equivalent to voluminous felsic plutons in the Limpopo belt (e.g. Berger et al., 1995; Mkweli et al., 1995; Kröner et al., 1999). The Matsitama granitoids are also coeval to the Vumba granitoids (Bagai et al., 2002) and to Upper Bulawayan greenstone belts and Sesombi granitoid suites in the Zimbabwe craton (Wilson et al., 1995; Luais and Hawkesworth, 1994; Jelsma et al., 1996).

The Tati granite–greenstone terrane (Fig. 2) includes the Tati greenstone belt, voluminous granitoids and gabbros, and minor metasedimentary rocks (e.g. Key et al., 1976; Tombale, 1992). Preliminary U–Pb zircon geochronological data (Kampunzu, unpublished) and the continuation of granitoid bodies from Francistown (Tati terrane) up to the Vumba granite–greenstone terrane suggest similar emplacement ages (e.g. Key et al., 1976; Tombale, 1992), i.e. between ~ 2.73 and 2.65 Ga (Bagai et al., 2002). Ten main intrusive complexes were identified in the Tati gran-

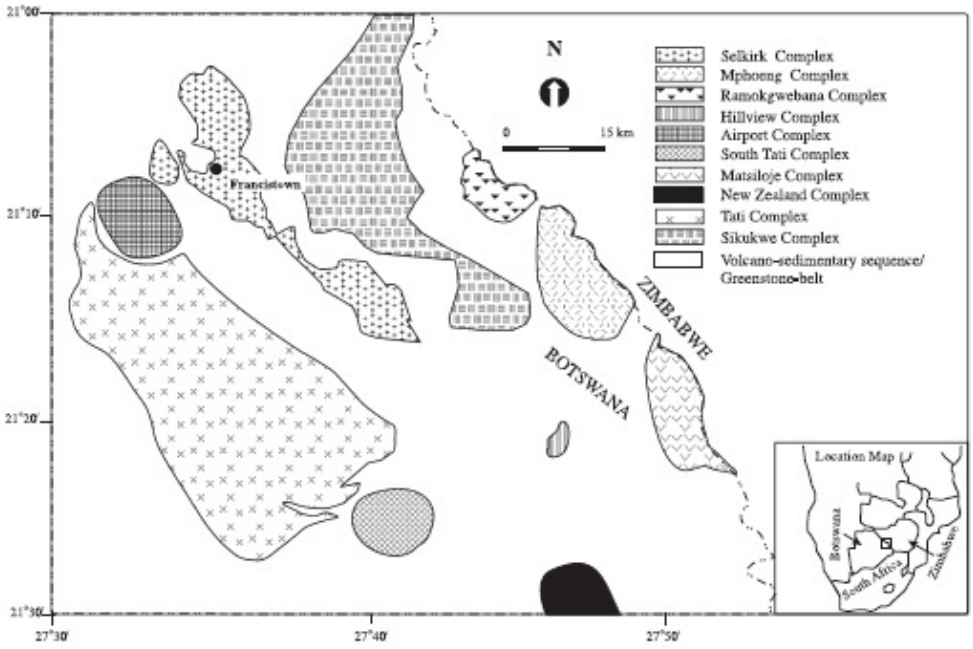

Fig. 2. Simplified map outlining the main intrusive bodies of the Tati granite–greenstone terrane (modified from Tombale, 1992). Insert: Location of the main map in southern Africa.

ite–greenstone terrane (Fig. 2). Four (Mphoeng, Ramokgwebana, Matsiloje and Sekukwe) are located northeast of the Tati greenstone belt and extends into Zimbabwe to the east and northeast. This group is referred to as the northeastern igneous complexes. The Ramokgwebana granitoids include coarse to porphyritic granites made of K-feldspar (megacrystic), quartz, biotite, amphibole, zircon and titanite. The Matsiloje batholith is made of coarse tonalites and trondhjemites. The Mphoeng complex consists of coarse to porphyritic gabbros, tonalites and trondhjemites. The gabbros consist of plagioclase in a dark coarse-grained groundmass of pyroxene, plagioclase, minor hornblende, biotite and opaque minerals. TTGs exposed in the northeastern igneous complexes are large bodies preserving igneous fabrics, except along discrete shear zones. These rocks are equigranular and contain plagioclase, quartz, amphibole, biotite, zircon, titanite, apatite and magnetite. The southwestern igneous complexes, located southwest of the Tati greenstone belt, include the Tati complex (Fig. 2) and its satellites called Airport, South Tati and New Zealand complexes which intrude the Tati greenstone belt lithologies. The most important lithologies in the southwestern igneous complexes are coarse grey tonalites, trondhjemites and granites converted into orthogneisses (Tombale, 1992). Tonalite and trondhjemite of the southwestern complex are foliated to banded grey gneisses (Martin, 1994) containing orthoamphibolitic enclaves. The main fabric in these rocks trend NW–SE. The most frequent minerals in these gneisses are plagioclase, quartz, biotite, amphibole, titanite, epidote, zircon, magnetite and apatite. Microcline occurs in some samples. In the southwestern igneous complexes, an intense tectonic foliation occurs close to the Limpopo–Shashe belt. Foliated pink K-feldspar megacrystic granites and granite dykes intruding the southwestern igneous complex close to the Limpopo–Shashe belt could be linked to the evolution of that belt. These granites were excluded from this study that is focused on the evolution of the Zimbabwe craton. The central igneous complexes include Selkirk and Hillview complexes. The Selkirk complex is elongated NW–SE, parallel to the trend of the Tati greenstone belt. The absence of a pervasive NW–SE solid-state fabric in this complex suggests that it post-dates the emplacement of the southwestern igneous complexes. It includes troctolites, gabbros and diorites intruding the Tati greenstone belt lithologies. The primary minerals in these rocks include plagioclase, olivine, pyroxene and opaque minerals. The Ni–Cu sulphide deposits of Selkirk and Phoenix mines are hosted in this complex.

3. Sampling and analytical techniques

Hundred rock samples selected for geochemical analyses were collected from mine drillcores and from large grey gneiss complex outcrops where the least altered and deformed rocks are exposed. We also sampled plutonic bodies preserving igneous mineralogy and/or igneous foliation in the northern and central complexes. The locations of the samples used in this study are compiled on the new 1/125,000 map of the Botswana Geological Survey Department (Francistown Quarter Degree sheet, to be published in 2003).

Samples with initials AR were analysed at Memorial University of Newfoundland (Canada). Major element compositions were determined using a Perkin Elmer (except for P_2O_5: colourimetry) and trace elements Rb, Sr, Ga, Zr, Y, Nb, Th, U, Pb, Zn, V, Cr and Ni were analysed using a Philips 1450 XRF. The other trace elements, including REE, were determined using an ICP-MS (Jenner et al., 1990). The remaining samples were analysed at Chemex laboratories (Canada) using ICP-AES (major elements) and ICP-MS (trace elements), except Li, Cr, Pb and Ni, which were determined using AAS. The precision for all the chemical analyses is better than 1% for major elements and better than 5% for trace elements. Representative analyses of the main intrusive rock-types are listed in Table 1. Several samples yielded relatively high LOI values, reflecting the alteration of the rocks. However, the variation trends and concentrations of major elements, high-field-strength elements (HFSE), REE and transition metals are similar to modern plutonic rocks and are thought to reflect primary magmatic distributions. Alkalies show some scatter and were probably slightly modified by secondary processes in some samples and REE contents of some samples (e.g. NN6 and NN8) show abnormal low values correlating with petrographic features (e.g. sericitisation) suggesting that these samples were affected by hydrothermal alteration. These rocks were

Table 1

	Sanukitoid suite									TTG suite					
	Gabbros				High-Mg diorites					Enclaves		Tonalites–Trondjhemites–Na-granites			
	MK115	AR227	TS86	TS163	AR128	AR234	AR71	AR243	MK32	AR77	AR78	TS169	MK83	AR63	MKQ3
SiO_2	44.00	48.80	49.84	49.33	52.40	53.10	53.40	56.50	59.00	48.90	51.10	60.59	61.77	62.22	67.33
TiO_2	0.09	0.50	0.21	0.11	0.52	0.36	0.28	0.36	0.55	1.63	1.24	0.75	0.73	0.91	0.58
Al_2O_3	26.00	21.70	18.66	16.59	14.30	17.30	16.20	17.20	10.75	14.00	14.01	14.80	14.27	15.71	15.06
Fe_2O_3	4.33	0.71	7.23	7.78	0.98	0.59	0.65	0.58	8.32	1.34	1.59	4.38	6.08	0.71	4.31
FeO		5.71			7.90	4.78	5.28	4.66		10.81	12.87			5.77	
MnO	0.06	0.11	0.13	0.14	0.17	0.08	0.11	0.08	0.13	0.17	0.19	0.06	0.09	0.12	0.06
MgO	8.98	4.88	7.82	8.11	7.39	7.74	7.63	7.74	8.02	4.49	4.18	3.15	3.14	3.38	1.41
CaO	15.69	13.08	13.80	13.34	7.76	6.66	12.94	6.66	8.84	10.60	8.10	7.41	5.45	5.23	4.03
Na_2O	1.10	1.85	1.60	1.43	3.82	2.42	1.80	2.42	2.33	2.90	2.93	6.17	3.63	3.74	4.24
K_2O	0.07	0.14	0.14	0.10	0.20	2.31	0.13	2.31	0.78	0.36	3.38	0.19	1.96	2.02	2.01
P_2O_5	0.01	0.03	0.01	0.01	0.08	0.14	0.04	0.14	0.08	2.15	1.93	0.18	0.26	0.15	0.16
LOI	1.75	1.94	1.41	1.52	1.76	2.27	1.06	2.33	0.88	0.47	3.76	2.88	0.88	0.88	0.58
Total	100.08	99.46	100.85	99.36	97.28	97.75	99.52	100.98	99.73	97.82	99.28	100.56	98.26	100.88	99.77
Mg#	0.80	0.57	0.68	0.68	0.60	0.72	0.69	0.72	0.65	0.40	3.34	0.59	0.51	0.48	0.39
Cr	694		16.0	24.0	234	108		194	118		74.0	29.0	52.0		12.0
Ni	270		26.0	32.0	81.0	340		339	48.0		2.0	6.0	43.0		10.0
Co	41.5		45.5	50.0					43.0			13.5	27.5		21.5
V			125	115	248	76.0		73.0	165		145	95.0	105		55.0
Cu	5.0		80.0	75.0	16.0	53.0		53.0	65.0		5.0	5.0	20.0		5.0
Pb	1.0	0.5	1.0	1.0		16.0	1.6	16.0	2.0		1.0	1.0	3.0		3.0
Zn	15.0		25.0	30.0	51.0	46.0		56.0	55.0		83.0	35.0	75.0		60.0
Rb	2.20	3.11	2.80	4.30	2.00	115	2.00	116	19.40	10.00	12.00	2.60	97		70.6
Cs	0.60	0.31	0.20	0.10	0.05	5.50	0.10	5.66	0.33	0.26		0.40	11.60	5.92	2.50
Ba	16.0	35.0	69.5	72.0	27.0	490	61.0	504	139	136		465	458	350	708
Sr	100	143	214	184	151	251	177	252	136	229	218	244	352	298	296
Li	1.0	12.0	3.0	4.0	6.1	29.0	7.6	32.2	6.0	8.7		3.0	31.0	191	25.0
Ta	1.00	1.11	2.00	1.50	0.10	0.76	0.08	0.75	3.00	0.26		2.50	4.00	0.55	5.50
Nb	1.00	0.97	1.00	1.00	3.00	4.00	1.00	5.00	4.00	3.29	5.00	7.00	8.00	6.28	11.00
Hf	1.00		1.00	1.00					3.00			5.00	4.00	0.00	5.00
Zr	1.00	8.00	10.00	7.50	45.00	108	16.00	111	99.5	33.5	81.0	169	195	65	207
Y	2.00	8.00	5.00	6.00	19.00	7.00	7.00	6.00	14.00	26.80	29.00	23.50	18.50	21.25	22.50
Th	2.00	0.20	1.00	1.00	1.00	20.00	0.80	18.00	6.00	2.20	1.00	3.00	7.00	3.20	6.00
U	0.50		0.50	0.50	0.30	6.00	0.20	5.00	2.00	0.70		0.50	3.00	2.07	3.00
La	1.00	1.61	2.50	3.00	3.30	34.13	4.00	23.80	12.00	21.10		16.50	35.00	26.15	45.5
Ce	1.50	4.00	4.50	5.00	7.89	46.66	8.10	44.77	25.53	45.81		36.5	65.0	41.6	85.5
Pr	0.20	0.60	0.70	0.70	1.09	5.28	1.00	5.07	3.13	6.13		4.60	8.00	5.86	8.90
Nd	1.00	2.87	3.00	3.50	5.04	19.03	4.14	18.48	12.00	27.57		18.50	28.50	23.12	31.00
Sm	0.20	1.00	0.70	0.90	1.56	3.41	1.00	3.37	2.90	6.16		4.00	4.90	4.60	5.70
Eu	0.10	0.47	0.40	0.60	0.50	0.74	0.41	0.77	0.90	2.10		1.30	1.50	1.45	1.50
Gd	0.30	1.28	1.10	1.10	2.14	2.91	1.19	3.13	2.80	6.94		5.00	4.90	4.40	6.50
Tb	0.10	0.22	0.10	0.10	0.38	0.33	0.18	0.30	0.50	0.89		0.70	0.80	0.65	0.80
Dy	0.30	1.47	1.00	1.10	2.59	1.67	1.16	1.78	2.80	5.23		4.60	4.30	3.87	4.50
Ho	0.10	0.31	0.10	0.20	0.59	0.32	0.25	0.31	0.50	1.00		1.00	0.60	0.78	0.80
Er	0.20	0.95	0.60	0.90	1.69	0.91	0.78	0.90	1.60	2.83		2.50	1.70	2.15	2.30
Tm	0.10	0.13	0.10	0.10	0.25	0.13	0.11	0.13	0.23	0.37		0.30	0.30	0.31	0.30
Yb	0.10	0.88	0.50	0.50	1.68	0.75	0.77	0.75	1.33	2.25		2.20	2.10	1.95	2.00
Lu	0.10	0.13	0.10	0.10	0.24	0.12	0.11	0.12	0.23	0.35		0.30	0.20	0.25	0.30

Except in samples with initial AR, Fe_2O_3 represents total iron.

excluded from the geochemical diagrams and the discussion of results. In the text, the compositions used when describing individual samples were recalculated to 100% anhydrous to minimise the effect of alteration on the samples.

4. Geochemical classification

The chemical analyses illustrate that the rocks exposed in the Francistown plutonic complex range from gabbros to granites (Table 1). The chemical

MK80	TS2	MKQ4	MK104	MK68	AR150	AR60	NN82B	AR188	TS168A	TS168B	MK36	AR181	MKQ2	TS167	MK34B
67.57	68.10	68.13	68.40	68.50	69.30	69.62	70.00	71.10	71.21	71.61	72.50	72.90	73.50	73.82	73.86
0.57	0.51	0.53	0.40	0.66	0.40	0.73	0.19	0.34	0.16	0.19	0.21	0.16	0.23	0.28	0.16
13.77	15.86	15.03	15.58	13.17	16.00	14.25	16.68	15.30	15.07	15.30	13.46	13.00	13.65	11.49	13.84
4.19	3.34	3.18	3.12	4.43	0.22	0.46	1.06	0.12	1.58	1.43	2.04	0.14	2.15	4.68	1.49
					1.79	3.70		0.99				1.12			
0.06	0.05	0.03	0.04	0.05	0.03	0.06	0.02	0.03	0.02	0.01	0.03	0.04	0.03	0.06	0.03
1.08	1.06	1.11	1.33	0.76	0.74	1.68	0.43	0.56	0.47	0.52	0.47	0.42	0.49	0.15	0.45
2.69	3.49	4.16	3.56	2.54	2.20	3.72	3.35	2.32	1.72	1.34	2.56	1.24	2.52	1.56	2.28
4.81	4.87	4.46	4.62	4.23	4.86	4.12	5.11	4.84	5.62	5.37	4.49	4.04	4.49	4.04	3.86
1.85	1.59	1.46	2.14	2.56	3.56	1.51	2.47	2.28	1.73	1.81	2.10	2.86	1.64	1.63	2.60
0.16	0.18	0.18	0.09	0.20	0.19	0.17	0.05	0.13	0.04	0.05	0.05	0.02	0.04	0.03	0.01
1.86	0.63	0.61	0.69	1.80	0.46	0.53	0.97	1.02	1.42	1.42	0.64	2.93	0.36	1.02	1.82
98.61	99.68	98.88	99.97	98.90	99.75	100.53	100.33	98.93	99.04	99.05	98.55	98.87	99.10	98.76	100.40
0.34	0.39	0.41	0.46	0.25	0.40	0.42	0.45	0.48	0.37	0.42	0.31	0.38	0.31	0.60	0.37
14.0	9.0	9.0	22.0	7.0	21.0	62.6	8.0	18.0	6.0	7.0	7.0	14.0	6.0	6.0	20.0
6.0	10.0	10.0	12.0	1.0	8.0	17.2	4.0	11.0	2.0	4.0	1.0	6.0	3.0	1.0	2.0
15.5	13.5	16.5	15.0	19.5		0.0	16.0		10.5	11.5	22.5		16.0	14.0	18.5
45.0	25.0	35.0	45.0	40.0	30.0	70.7	15.0	13.0	10.0	15.0	15.0	8.0	5.0	5.0	10.0
5.0	5.0	5.0	20.0	5.0	19.0	11.1	5.0	15.0	5.0	15.0	5.0	34.0	5.0	5.0	20.0
7.0	2.0	1.0	4.0	10.0	22.0	8.1	18.0	19.0	4.0	3.0	7.0	18.0	3.0	3.0	1.0
110	85.0	80.0	50.0	105	63.0	60.6	25.0	49.0	35.0	30.0	90.0	39.0	60.0	40.0	25.0
177	104	67.8	62.2	119.0	102.0	87.0	63.0	75.0	51.0	55.0	83.0	144	76.4	40.2	101
4.60	3.50	3.20	2.40	1.50	1.52	4.72	2.00	3.49	1.10	1.00	2.40	1.73	2.90	0.30	1.70
342	212	421	628	1210	1007	449	789	1232	756	459	358	543	247	905	943
179	228	325	397	280	493	260	501	430	402	223	222	101	162	89	177
60.0	35.0	31.0	24.0	21.0	24.4	108	19.0	54.4	4.0	5.0	21.0	3.6	25.0	3.0	2.0
5.50	4.00	4.50	2.50	4.00	0.33	0.66	5.00	0.31	2.50	3.50	8.00	1.23	6.00	5.50	5.50
29.00	12.00	9.00	3.00	12.00	4.00	9.09	1.00	3.00	2.00	2.00	10.00	9.00	9.00	13.00	6.00
13.00	5.00	5.00	3.00	11.00			1.00		2.00	2.00	4.00	3.00		4.00	9.00
445	215	235	108	458	163	202	79	116	72	83	123	91	150	304	108
75.5	11.00	7.00	6.00	17.50	2.00	17.18	2.50	1.00	3.50	6.50	9.50	18.00	7.00	39.0	12.00
38.00	5.00	4.00	5.00	21.00		12.12	2.00	2.00	1.00	1.00	4.00	11.00	4.00	7.00	17.00
4.50	5.00	3.00	1.50	1.50	4.00	1.01	1.50	0.90	1.00	0.50	5.00	3.00	3.50	3.00	3.50
167	31.5	30.00	18.50	143	26.57	51.5	7.50	10.66	9.00	18.50	20.50	14.24	39.0	36.5	26.50
373	56.5	54.5	35.5	263	49.4	78.3	14.0	20.0	14.5	17.5	33.5	27.2	62.5	72.5	47.5
42.10	6.50	5.60	4.00	27.7	5.30	9.08	1.70	2.42	2.00	3.50	3.70	2.94	6.50	8.50	4.60
160	21.50	20.50	15.50	89.5	18.50	30.9	7.00	8.40	5.50	12.00	12.50	1.68	19.50	32.00	15.50
32.30	3.60	3.20	2.90	11.60	2.95	5.09	1.20	1.57	1.30	2.70	2.20	2.46	3.20	6.30	3.00
2.20	0.80	0.90	0.80	1.80	0.81	1.36	0.40	0.41	0.40	0.70	0.60	0.47	0.50	1.00	0.60
30.50	3.70	4.40	2.00	10.40	2.48	4.48	1.10	1.27	1.10	2.10	2.30	2.86	2.70	6.40	3.10
4.20	0.60	0.30	0.30	1.10	0.21	0.60	0.10	0.11	0.10	0.30	0.30	0.43	0.30	1.00	0.40
20.50	2.60	2.00	1.30	5.10	0.97	3.37	0.50	0.60	0.60	1.40	2.10	2.68	1.40	7.40	2.20
3.40	0.30	0.20	0.30	0.60	0.15	0.66	0.10	0.10	0.10	0.30	0.30	0.54	0.20	1.40	0.40
7.20	1.30	0.50	0.70	1.60	0.41	1.77	0.20	0.21	0.30	0.60	1.20	1.70	1.10	4.30	1.10
0.90	0.10	0.10	0.10	0.30	0.06	0.24	0.10	0.04	0.10	0.10	0.10	0.26	0.10	0.70	0.10
5.00	0.80	0.60	0.50	1.20	0.33	1.59	0.20	0.21	0.40	0.50	0.80	1.80	0.80	4.20	1.10
0.70	0.10	0.10	0.10	0.10	0.05	0.25	0.10	0.03	0.10	0.10	0.20	0.27	0.10	0.60	0.10

(continued on next page)

compositions define three distinct petrological suites. The first suite includes rocks defining a tonalite–trondhjemite–granite association, hereafter called TTG suite (Fig. 3a). The MgO content in the TTG suite is <5 wt.%, and Mg# ($Mg/(Mg+Fe^{2+})$) calculated with $Fe^{3+}/Fe^{2+}=0.2$ is ≤ 0.5, including in ortho-amphibolitic enclaves hosted in the trondhjemites and marked by $SiO_2<53\%$ (e.g. sample AR77, Table 1). The Al_2O_3 content of TTG rocks containing SiO_2 in the range 67–73% defines two groups. The

Table 1 (*continued*)

	TTG suite							High-K granite suite								
	Tonalites–Trondhjemites–Na-granites							Potassic granites								
	MKQ1	TS82	TS79	BR24A	MK43A	MK43B	TS168C	MK54	MK108	MKQDK1	MK112A	MK49	NN8	MKQ5	NN6	MK19
SiO_2	74.00	74.39	74.46	74.50	75.22	76.00	77.01	70.73	71.86	72.20	73.50	74.27	75.82	76.50	76.50	77.58
TiO_2	0.13	0.08	0.26	0.06	0.03	0.06	0.04	0.28	0.22	0.28	0.21	0.01	0.04	0.06	0.03	0.04
Al_2O_3	14.09	13.53	10.94	13.86	13.53	14.20	12.94	13.57	13.11	13.47	12.65	12.60	13.65	12.70	13.27	12.41
Fe_2O_3	1.37	1.36	3.06	0.85	0.70	0.75	0.86	2.25	1.84	2.42	1.61	0.45	0.46	0.76	0.44	0.63
FeO																
MnO	0.02	0.04	0.06	0.01	0.01	0.01	0.01	0.04	0.02	0.02	0.02	0.01	0.02	0.01	0.01	0.01
MgO	0.27	0.20	0.12	0.33	0.07	0.16	0.10	0.55	0.47	0.39	0.29	0.05	0.17	0.11	0.13	0.21
CaO	2.01	1.28	1.11	1.91	1.29	1.65	0.47	1.66	1.71	1.33	1.03	0.44	0.99	1.15	0.95	1.36
Na_2O	4.32	4.40	4.14	5.17	4.55	4.56	3.65	3.65	4.07	3.03	3.21	2.53	3.46	3.27	3.58	3.22
K_2O	3.09	3.04	2.22	1.80	3.10	2.86	3.51	4.51	4.17	5.74	5.07	7.70	4.52	5.60	4.82	4.47
P_2O_5	0.01	0.03	0.11	0.02	0.01	0.01	0.01	0.08	0.07	0.06	0.04	0.01	0.01	0.01	0.01	0.01
LOI	0.53	1.67	1.00	0.68	0.41	0.38	0.82	1.39	0.64	0.87	0.73	0.36	0.47	0.31	0.73	0.90
Total	99.84	100.02	98.38	99.19	98.92	100.64	99.42	98.71	98.18	99.81	98.36	98.43	99.59	100.48	100.47	100.84
Mg#	0.28	0.23	0.70	0.43	0.17	0.30	0.19	0.33	0.34	0.24	0.26	0.18	0.42	0.22	0.37	0.40
Cr	5.0	4.0	5.0	26.0	26.0	46.0	4.0	8.0	7.0	5.0	6.0	6.0	12.0	3.0	10.0	14.0
Ni	3.0	7.0	3.0	15.0	5.0	13.0	1.0	7.0	7.0	3.0	7.0	1.0	3.0	7.0	1.0	14.0
Co	19.0	9.0	15.5	12.5	12.5	16.0	16.0	13.5	14.0	15.0	9.0	26.5	23.0	16.0	24.5	9.5
V	5.0	5.0	5.0	5.0	5.0	5.0	5.0	20.0	15.0	5.0	15.0	5.0	5.0	5.0	5.0	5.0
Cu	5.0	5.0	5.0	10.0	5.0	5.0	35.0	5.0	5.0	5.0	5.0	15.0	5.0	35.0	5.0	10.0
Pb	5.0	15.0	4.0	16.0	21.0	15.0	4.0	18.0	15.0	19.0	11.0	4.0	11.0	7.0	17.0	4.0
Zn	45.0	40.0	40.0	15.0	5.0	10.0	5.0	60.0	55.0	55.0	35.0	5.0	5.0	5.0	5.0	10.0
Rb	99.2	86.0	48.0	24.2	93.4	62.2	61.8	149	172	198	297	202	115	145	117	114
Cs	2.40	2.00	0.30	0.40	0.50	0.40	0.20	0.80	1.80	1.40	4.70	1.20	1.20	1.50	1.00	1.60
Ba	570	751	984	679	535	693	1010	966	838	1085	706	1835	1115	1765	1040	1055
Sr	168	128	75	196	120	184	82	180	189	124	101	280	184	154	178	151
Li	16.0	7.0	3.0	1.0	1.0	1.0	1.0	14.0	15.0	26.0	11.0	2.0	3.0	7.0	3.0	7.0
Ta	8.50	3.00	6.00	5.00	4.50	6.00	7.00	4.00	5.50	5.50	5.50	8.50	7.00	6.50	8.00	4.00
Nb	9.00	5.00	14.00	6.00	1.00	6.00	9.00	10.00	12.00	11.00	13.00	2.00	3.00	4.00	2.00	3.00
Hf	3.00	2.00	9.00	1.00	4.00	1.00	4.00	7.00	6.00	8.00	6.00	1.00	3.00	1.00	1.00	1.00
Zr	94	43	292	57	117	58	81	222	182	276	183	25	93	65	66	29
Y	9.00	6.00	35.5	8.00	11.00	11.50	18.50	16.50	9.50	19.00	17.00	3.50	1.50	5.00	1.50	4.00
Th	4.00	3.00	6.00	11.00	49.0	13.00	9.00	25.00	22.00	37.00	27.00	1.00	1.00	4.00	2.00	13.00
U	7.00	2.50	3.00	2.50	5.00	2.50	5.50	7.50	8.00	6.50	4.00	0.50	3.00	19.00	3.00	4.50
La	21.50	13.00	32.00	18.50	48.5	22.00	9.50	76.5	69.5	113	9.00	9.00	2.50	16.00	2.50	5.50
Ce	35.0	24.0	64.0	32.0	87.5	38.0	28.5	142	122	223	80.0	15.0	5.0	27.5	3.5	13.5
Pr	3.50	2.70	7.20	3.00	8.80	3.70	2.40	15.10	12.20	23.80	2.10	2.10	0.40	2.90	0.40	1.20
Nd	12.50	11.00	27.50	9.50	30.00	12.00	8.00	47.00	42.00	79.00	7.00	5.50	1.50	10.00	1.50	4.50
Sm	2.30	2.10	5.90	1.80	5.00	2.00	1.80	7.90	6.10	10.60	1.50	1.80	0.60	2.00	0.30	3.80
Eu	0.80	0.50	1.10	0.60	0.70	0.60	0.30	0.80	0.80	1.20	0.30	0.60	0.50	0.50	0.40	3.50
Gd	2.10	1.50	6.40	1.60	3.80	2.00	2.50	8.40	5.60	11.10	2.50	1.20	0.40	1.90	0.30	1.00
Tb	0.30	0.20	1.00	0.30	0.60	0.30	0.50	1.00	0.60	1.20	0.40	0.20	0.10	0.20	0.10	3.10
Dy	2.20	1.10	6.50	1.20	2.10	1.80	3.20	4.10	2.50	4.50	2.40	0.50	0.20	1.40	0.20	3.80
Ho	0.40	0.30	1.30	0.30	0.40	0.40	0.60	0.60	0.30	0.70	0.80	0.10	0.10	0.10	0.10	3.10
Er	1.10	0.90	4.10	0.70	1.00	1.10	1.80	1.60	0.90	2.20	2.10	0.50	0.10	0.70	0.20	3.50
Tm	0.10	0.10	0.70	0.10	0.10	0.10	0.40	0.30	0.10	0.30	0.30	0.10	0.10	0.10	0.10	3.10
Yb	0.80	0.40	4.00	1.00	1.10	1.20	2.00	1.40	0.70	1.70	2.20	0.40	0.30	0.80	0.20	3.50
Lu	0.10	0.10	0.70	0.10	0.10	0.20	0.40	0.10	0.10	0.30	0.40	0.10	0.10	0.10	0.10	3.10

first group (hereafter Group 1 TTG sub-suite) contains >15% Al_2O_3 indicating a high-Al trondhjemitic sub-suite, whereas the second group (hereafter Group 2 TTG sub-suite) has <15% Al_2O_3 and corresponds to a low-Al trondhjemitic sub-suite (Barker, 1979; Martin, 1993, 1994). The high-Al trondhjemitic sub-suite occurs in the southwestern igneous complexes whereas the low-Al trondhjemitic sub-suite forms the northeastern igneous complexes. In the diagram K_2O–Na_2O–CaO (Fig. 3b), the majority of the Francistown

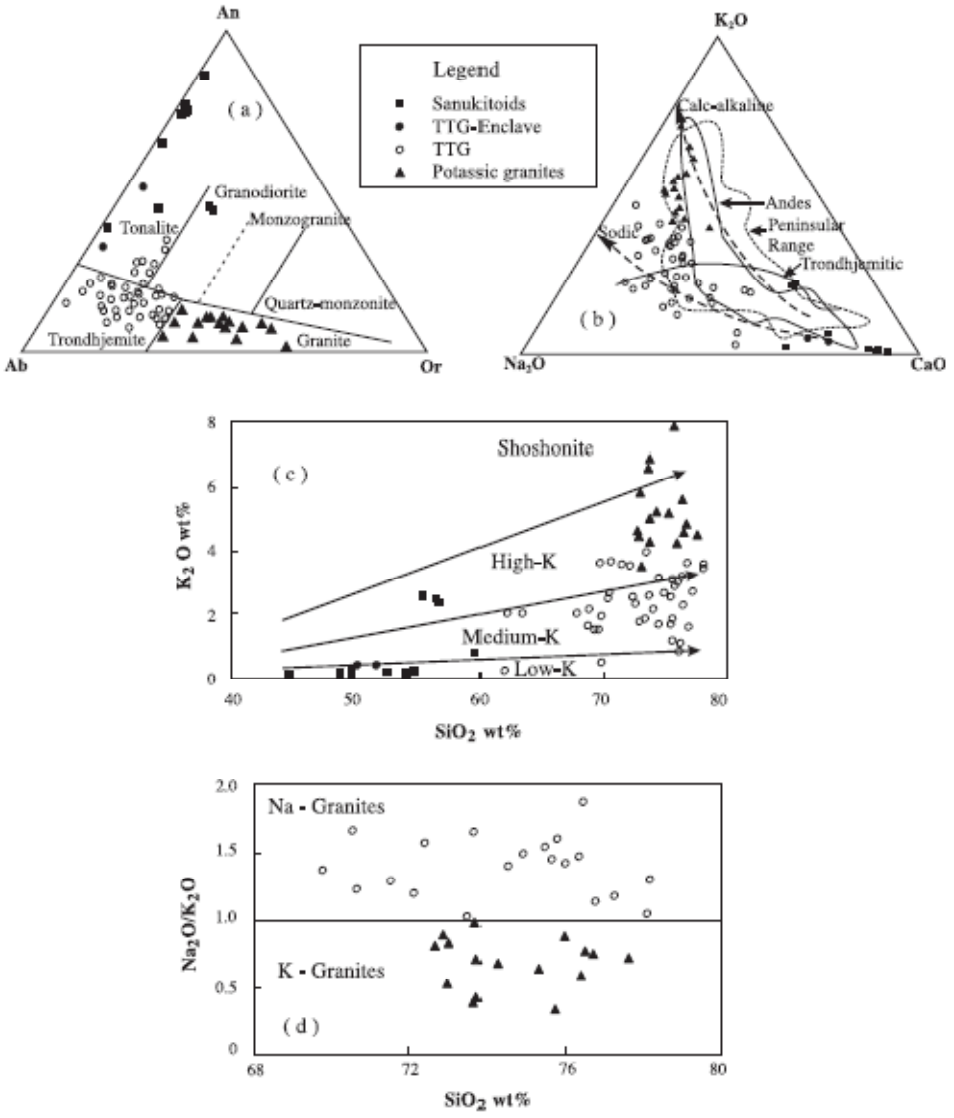

Fig. 3. Geochemical classification of the intrusive rocks from the Tati granite–greenstone terrane. (a) An–Ab–Or normative compositions; (b) K_2O–Na_2O–CaO diagram with the various fields and trends drawn according to Lunis and Hawkesworth (1994) and references therein; (c) K_2O–SiO_2 diagram with the fields drawn based on Gill (1981); (d) Na_2O/K_2O vs. SiO_2.

TTG suite rocks show similarities to arc granitoids in the Peninsular Range (Baird and Miesh, 1984). The most sodic samples plot along or close to the "sodic" TTG evolution trend as defined by Luais and Hawkesworth (1994).

The second igneous suite includes mafic and intermediate intrusive rocks (SiO_2: 45–60%) marked by high MgO contents (5–9.5%; Table 1) from the central igneous complexes. Similar high-Mg intermediate rocks were documented in other Archaean cratons, e.g. in the Superior Province in Canada where they represent ~15% of the late Archaean crust (Shirey and Hanson, 1984; Stern et al., 1989; Stern and Hanson, 1991; Stevenson et al., 1999). These high-Mg igneous suites were referred to as Sanukitoids (Shirey and Hanson, 1984) by reference to the Setouchi high-Mg andesites, Japan (Tatsumi and Ishizaka, 1982). The high-Mg andesites from the Japanese island arc have high Mg# (up to 0.7), similar to values recorded in Francistown Mg-diorite samples AR234, 237 and 245 (Table 1). The gabbro MK 115 from the central igneous complexes shows a higher Mg# (0.8). High-Mg intermediate rocks from the Canadian Superior Province have Mg# in the range 0.43–0.62. K_2O contents of mafic rocks (SiO_2 < 55%) of the Sanukitoid and TTG suites are similar in the Francistown complex. The rocks plot in the low-K field using Gill's (1981) discrimination boundaries (Fig. 3c). Intermediate and felsic rocks of the TTG suite plot in the medium-K field. The Mg-diorites of the Sanukitoid suite (e.g. samples AR45, 234 and 237; Table 1) show higher contents of K_2O and plot in the high-K domain (Fig. 3c). However, these rocks also have high Na_2O contents and Na_2O/K_2O ratios are >1 in mafic and intermediate rocks of both Sanukitoid and TTG suites. Trondhjemites show a large range of Na_2O/K_2O values, between 1.2 and 32, for silica contents between 62% and 77%. The highest Na_2O/K_2O ratios (32 and 19) are recorded in the trondhjemite TS169 and the dioritic Sanukitoid AR128, respectively.

The third igneous suite of intrusive rocks includes potassic granites (Na_2O/K_2O < 1; Fig. 3d), containing more than 72% SiO_2 and plotting in the high-K field (Fig. 3c). In the diagram $K_2O–Na_2O–CaO$ (Fig. 3b), the high-K granitoids plot also in the field defined by Peninsular Range arc granitoids (Baird and Miesh, 1984).

5. Geochemical variations

5.1. TTG suite

The most mafic rocks analysed (samples AR77 and 78; Table 1) are ortho-amphibolite enclaves with SiO_2 contents of 50% and 52%, respectively, and Mg# ~0.5. The sample AR 78 contains 74 ppm Cr and 2 ppm Ni. These values indicate that the protolith of these enclaves cannot represent a primary mantle-originating magma. There are no rocks with silica content between 52% and 62% in the TTG suite. Tonalites have Al_2O_3 contents between ~14% and 15.5% and TiO_2 concentrations between ~0.5% and 0.9% at ca. 63–69% SiO_2. The Al_2O_3 values compare to the average content reported by Martin (1993, 1994) for similar Archaean rocks whereas TiO_2 abundances in the Francistown rocks is slightly higher than the Archaean average for TTG suites. Major element compositions of the Francistown TTG rocks are shown in the Harker diagrams (Fig. 4). The rocks share a number of geochemical features with most Archaean TTG suites. They contain high Na_2O and the alumina saturation index (ASI = molecular ratio $Al_2O_3/(CaO + Na_2O + K_2O)$) is lower than one except in a few samples where it is in the range 1–1.1 (Fig. 5). These features along with the presence of amphiboles indicate a metaluminous composition. CaO, Na_2O and K_2O abundances show a wide range (Table 1) and there are correlations between K–Ba, K–Rb and CaO–Sr (Fig. 6).

HFSE show good correlation as shown in the diagrams Nb vs. Zr (Fig. 7a) and Zr vs. Hf (Fig. 7b) indicating an average Zr/Hf ratio of ~37 for the Francistown TTG suite which is similar to the average value of Zr/Hf in MORB and chondrite (~37 ± 2 ppm: David et al., 2000 and references therein).

The concentrations of incompatible trace elements (e.g. Rb, Ba, Sr, Nb, Zr and Th) increase from intermediate to felsic rocks, and the ratios of incompatible trace elements show a large range of composition, which partly originate from fractionation processes. However, some features are probably primary, e.g. Rb/Sr ratio of Group 1 TTG sub-suite is low (~0.5), similar to values typical for high-Al TTG sub-suites (Martin, 1993, 1994). Low-Al Group 2 TTG sub-suite displays variable Rb/Sr ratios in the range 0.4–1. Th/Ta ratio is ~8 in the enclave sample

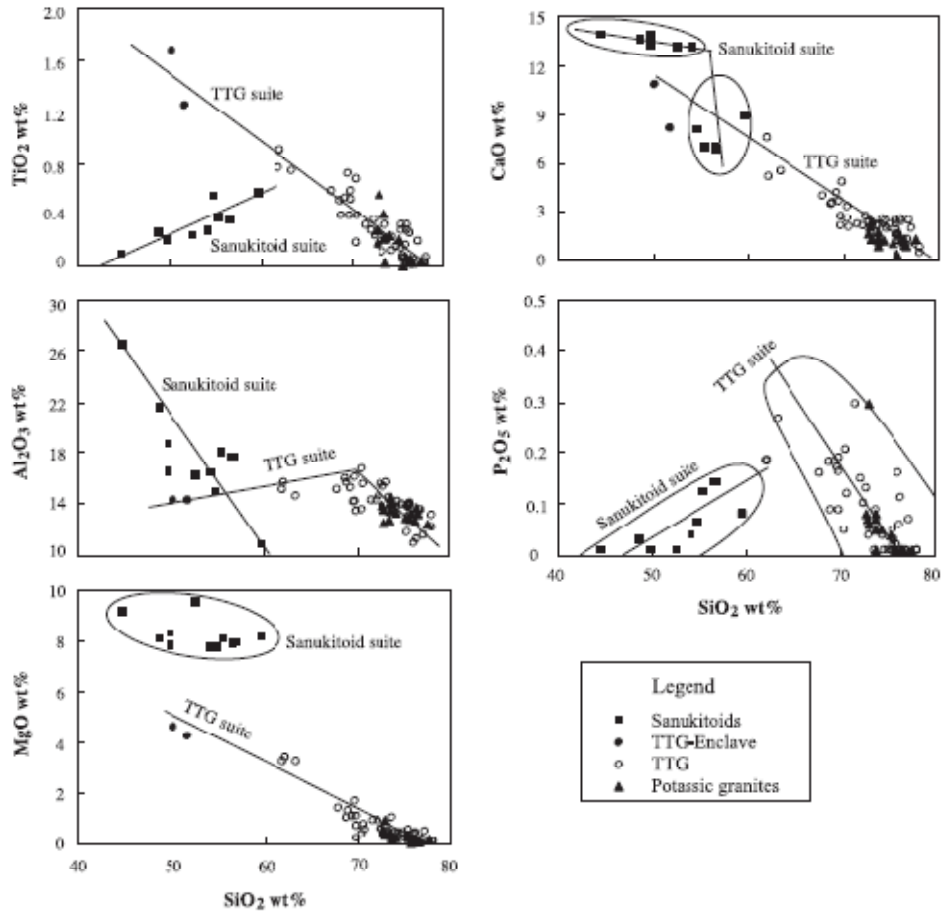

Fig. 4. Harker-type diagrams for intrusive rocks from the Tati granite–greenstone terrane.

AR 77 of mafic rocks contained in the Group 1 TTG rocks (SiO_2~ 50%). This enclave is also marked by a high value for La/Nb (~ 6) and a low Nb/Ta ratio (~ 13). These features are similar to those documented in arc mafic rocks (e.g. Sun and McDonough, 1989). Low Nb/Ta ratio (~ 13) in this sample of metamorphosed igneous mafic rock is similar to values reported in mafic rocks affected by retrograde hydration with fluids expulsed from a subducting slab (Kamber and Collerson, 2000).

Rb, Y, Nb, Th, Ta, Zr and Yb relationships in tonalites, trondhjemites and granites indicate also that the Francistown intermediate and felsic rocks are similar to equivalent igneous rocks in Phanerozoic arcs (Fig. 8a–c). High Th/Yb (>5) ratios correlated to high values (>10, up to ca. 100) for La/Yb show the

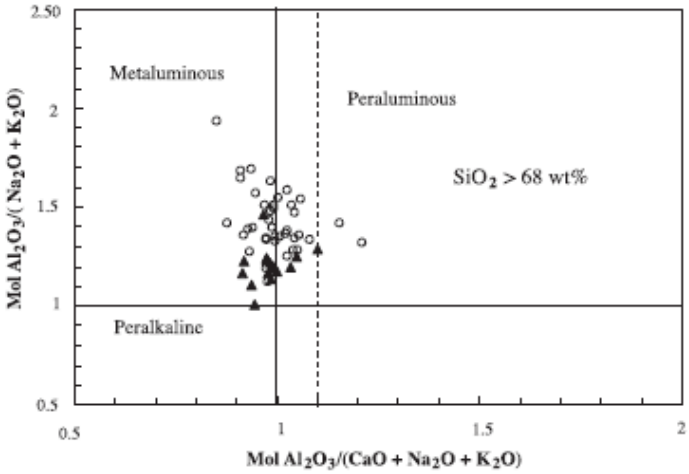

Fig. 5. Plot of $Al_2O_3/(Na_2O + K_2O)$ against ASI {molar $Al_2O_3/(CaO + Na_2O + K_2O)$} for intrusive felsic rocks from the Tati granite–greenstone terrane. Same symbols as in Fig. 3.

analogies of these intrusive rocks to modern continental arc felsic magmas (Fig. 8c). The Sr/Y ratio is variable, low in Group 2 TTG sub-suite rocks but reaches high values (Fig. 9a) typical of high-Al in Group 1 TTG sub-suite rocks. These analogies are also shown by the REE composition of the TTG suite shown in Fig. 9b.

The REE patterns of trondhjemites containing >70% SiO_2 discriminate the two TTG groups identified in the Francistown igneous complexes: (1) Group 1 TTG sub-suite rocks (e.g. samples AR 150, 188, BR24A, MK 34, 43B, TS 168B) are characterized by relatively low LREE contents (e.g. La_N: 33–83; Fig. 10c), low Yb_N: 1–5, La_N/Yb_N in the range 12–54 and the absence of significant Eu negative anomaly (Eu/Eu* = 0.9–1.1). Both LREE and HREE are fractionated as shown by La_N/Sm_N (4–7) and Gd_N/Yb_N (1.3–6; average = 3) ratios. These rocks share similarities with Archaean TTG which are characterised by $5 < La_N/Yb_N < 150$, $0.3 < Yb_N < 9$ and the lack of negative Eu anomaly (Martin, 1994); (2) Group 2 TTG sub-suite rocks (e.g. samples TS 70, 167, 168c, AR65, 81, 181) are marked by higher LREE contents (e.g. La_N up to 114), Yb_N up to ~ 20, lower La_N/Yb_N ratios in the range 3–10, and the REE patterns display significant negative Eu anomalies (Fig. 10e), with Eu/Eu* between 0.4–0.6. La_N/Sm_N ratios are in the range 3–6, whereas Gd_N/Yb_N is between 1 and 1.5 (average = 1.3). These rocks have affinities with post-Archaean arc granitoids. REE patterns of TTG suite rocks with SiO_2 between 62% and 70% are moderately fractionated (Fig. 10a) and similar to the high Na-granites of the first group (Martin, 1993, 1994). The analogies are supported by high ratios of La_N/Yb_N (up to 25), Gd_N/Yb_N (up to 3.2) and by the absence of significant negative Eu anomalies (Eu/Eu*: 0.8–1.0). The sample TS 80 (Fig. 10a) displays a positive Eu anomaly (Eu/Eu* = 1.4). Light REE are more fractionated ($La_N/Sm_N = 3–6$) than heavy REE ($Gd_N/Yb_N = 1–3$). The mafic enclave sample AR 77 from the TTG suite (Fig. 10g) is also enriched in REE (La_N ~ 66, Yb_N ~ 11 and La_N/Yb_N ~ 6) and shows fractionation for both LREE and HREE (La_N/Sm_N and Gd_N/Yb_N ~ 2). The absence of Eu anomaly is also characteristic for this sample (Eu/Eu* = 1). The relationships between La_N/Yb_N vs. Yb_N (Fig. 9b) suggest that Group 1 TTG sub-suite rocks have affinities with Archaean TTGs, whereas Group 2 TTG sub-suite rocks are similar to post-Archaean arc granitoids (Martin, 1993, 1994).

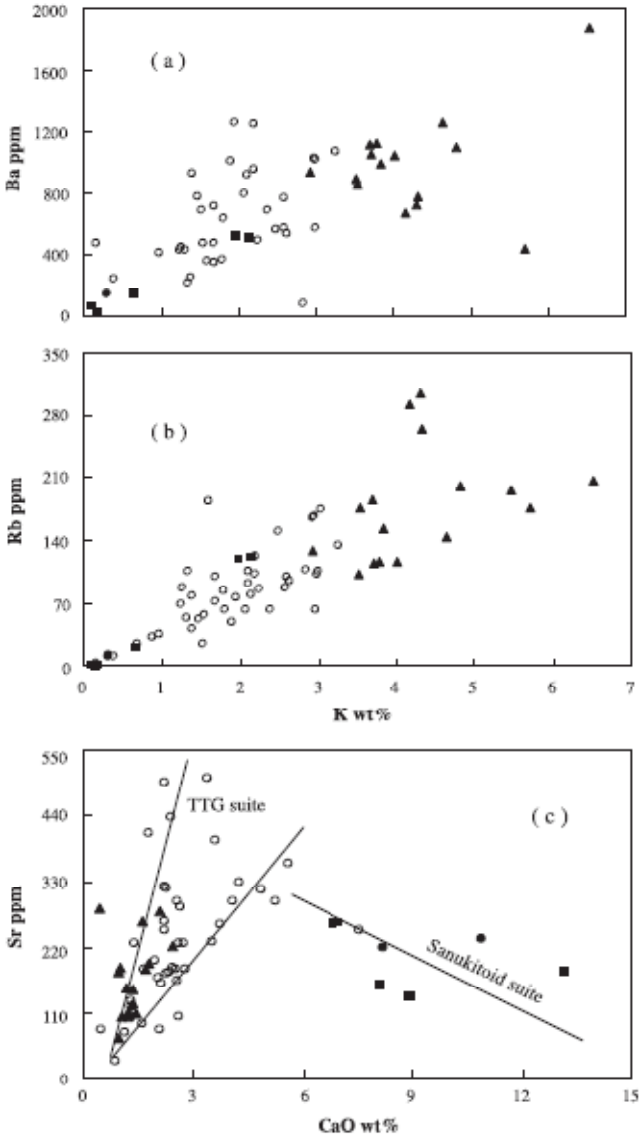

Fig. 6. Geochemical compositions of intrusive rocks from the Tati granite–greenstone terrane plotted in the binary diagrams: (a) Ba–K, (b) Rb–K, (c) Sr–CaO. Symbols as in Fig. 3.

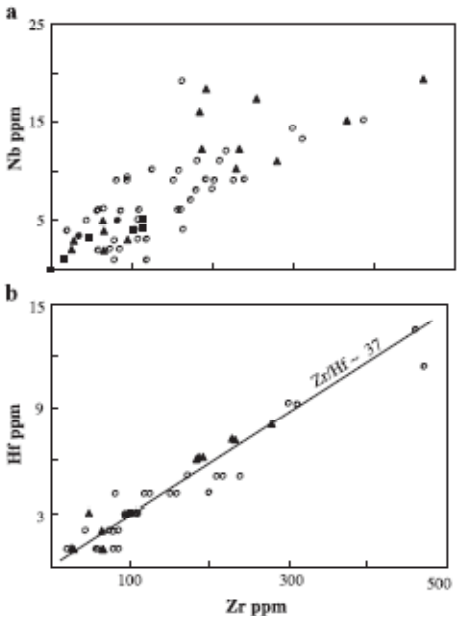

Fig. 7. High-field-strength-element compositions of intrusive rocks from the Tati granite–greenstone terrane plotted in the binary diagrams: (a) Nb vs. Zr, (b) Hf vs. Zr. Symbols as in Fig. 3.

Primordial mantle normalized plots (Fig. 11) summarize the distinctive features shared by all the igneous rocks of the TTG suite, i.e. negative anomalies for Ti and Nb (Ta). A negative anomaly for Sr and a positive anomaly for Hf (Zr) occur in Fig. 11e, within the Group 2 TTG rocks. Sr negative anomaly in primordial mantle normalised diagrams and flat chondrite-normalised HREE patterns are features indicating a non-adakitic composition of this group of TTG rocks. In contrast, the absence of a Sr anomaly and a small negative to no Hf anomaly (Fig. 11a and c) mark Group 1 TTG rocks. This group of rocks has adakitic affinities and this is supported by extremely high Sr/Y values (e.g. 430 in sample AR 188 and 250 in sample AR 150). These anomalies and the general shape of the primordial-mantle normalised spider diagrams are similar to the features of igneous rocks emplaced along convergent plate margins (e.g. Pearce, 1982; Pearce et al., 1984).

5.2. Sanukitoid suite

Al_2O_3 content in Sanukitoid mafic rocks (<53% SiO_2) is high, in the range ~16–26% (average ~20%), whereas the TiO_2 content is low (<0.3%). Similarly, high Al_2O_3 concentrations (16–18%, except

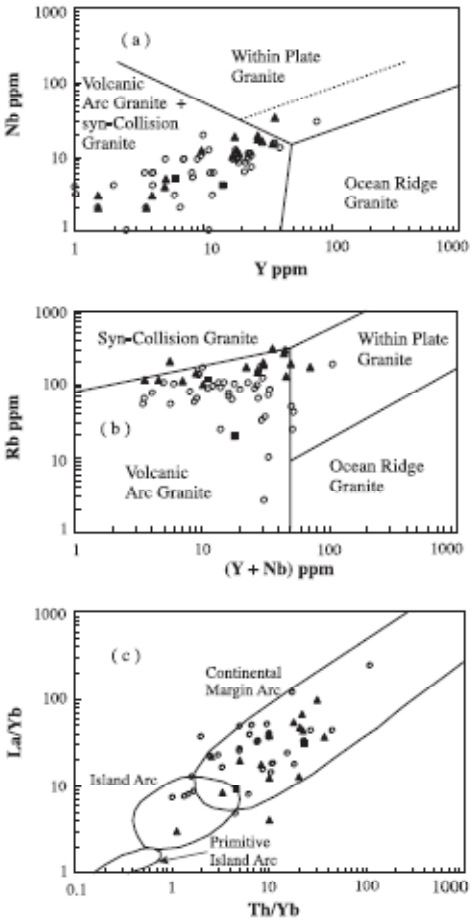

Fig. 8. Geochemical compositions of intrusive rocks from the Tati granite–greenstone terrane plotted in the tectonic setting discrimination diagrams: (a) Y vs. Nb, (b) Rb vs. Y+Nb (Pearce et al., 1984), (c) La/Yb vs. Th/Yb (Condie, 1989). Symbols as in Fig. 3.

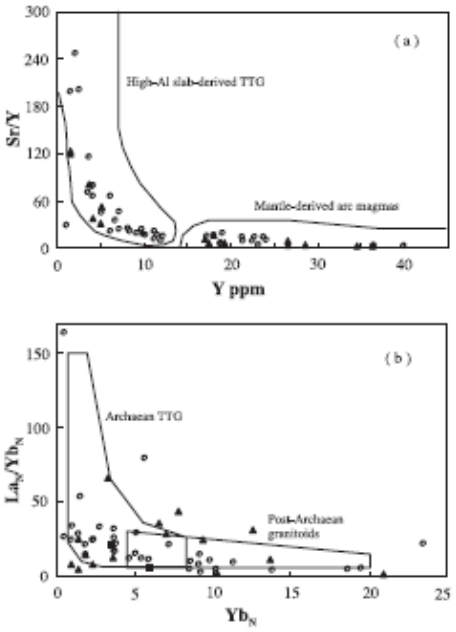

Fig. 9. Geochemical compositions of intrusive rocks from the Tati granite–greenstone terrane plotted in the diagrams: (a) Sr/Y vs. Y, (b) La_N/Yb_N vs. Yb_N. The fields are according to Martin (1993, 1994). Symbols as in Fig. 3.

in samples MK32 and AR128) and low TiO_2 abundances (<0.6%) occur in intermediate rocks (SiO_2: 54–60%). These features are similar to those marking high-Al mafic and intermediate magmas in modern arc settings (e.g. Gill, 1981; Thorpe, 1982). MgO contents are high in both mafic (5–9.5%) and intermediate (7.7–8.1%) rocks. The Mg# values are in the range 0.58–0.80. The highest Mg# (0.8) occurs in the gabbro MK115, which contains ~ 45% SiO_2. Diorites from this group have also high Mg# between 0.6 and 0.7. Within the Sanukitoid suite, the sample MK 115 contains the lowest SiO_2 content (~ 45%) correlated to the lowest abundances of most incompatible elements, e.g. Ba, Sr, Zr, Y and REE (Table 1). In contrast, it shows the highest content in Ni (280 ppm) and Cr (706 ppm) suggesting that it is representative of the most primitive magmas in this igneous suite. However, except for the most primitive gabbro MK 115, the transition metal abundances are generally higher in the Mg-diorites than in the gabbros of the Sanukitoid suite. The Mg-diorites of the Sanukitoid suite display higher contents of most incompatible trace elements (e.g. HFSE and REE) when compared to the gabbros of the same suite. Incompatible element ratios show a large range of values in the Sanukitoid suite. Th/Ta ratios are low (0.2–3, average ~ 1) in the mafic rocks, similar to values reported in mafic rocks emplaced in extensional tectonic settings such as MORB and OIB (e.g. Wood et al., 1979). High-Mg diorites show a very large range for Th/Ta values (2–26, average ~ 14). The high Th/Ta values compare to ratios in arc magmas (Wood et al., 1979). La/Nb values display a similar trend with low ratios (1–3; average ~ 2) similar to values recorded in average MORB and OIB worldwide (e.g. Sun and McDonough, 1989). A broader La/Nb range (1–6) and a higher average (~ 4) similar to La/Nb ratios in arc magmas characterise high-Mg diorites. Nb/Ta ratio is extremely variable in the Francistown Sanukitoid suite, but low values (<13) predominate, except in the high-Mg diorite sample AR 128 (Nb/Ta~ 30). Nb/Ta ratios in MORB and OIB and chondrites are ~ 17 ± 2 (e.g. Kamber and Collerson, 2000 and references therein). Sedimentary rocks and continental crust are marked by lower Nb/Ta values of ca. 12 ± 2. Blueschist- and eclogite-facies mafic rocks from obducted oceanic crust show a large Nb/Ta range, between 7 and 77, with an average of ~ 34 ± 4 (Kamber and Collerson, 2000).

Cs/La (0.08–0.6; average 0.24), Ba/Th (70–174, except in sample MK 115) and Ba/La (16–28; average 23) ratios are generally higher in mafic rocks than in high-Mg diorites (Cs/La: 0.02–0.24, average 0.11; Ba/Th: 23–76 and Ba/La 8–21, average 15). MORB and OIB are usually characterized by Cs/La<0.04, Ba/Th<100 and Ba/La<10 (e.g. Sun and McDonough, 1989). Higher ratios commonly occur in arc magmas (e.g. Gill, 1981; Ryan et al., 1995), especially at the volcanic arc front. For example, in the Central American arc, Cs/La>0.1 occur only at and close (<30 km) to the volcanic arc front, whereas this ratio is lower (<1, with most data <0.05) in igneous rocks emplaced behind the volcanic arc front (Walker et al., 2000). Ce/Pb ratio is low in both mafic (2–8) and high-Mg diorites (3–13) of the Francistown Sanukitoid suite. The Ce/Pb ratios of these rocks are similar to values marking arc magmas (e.g. Chauvel et al.,

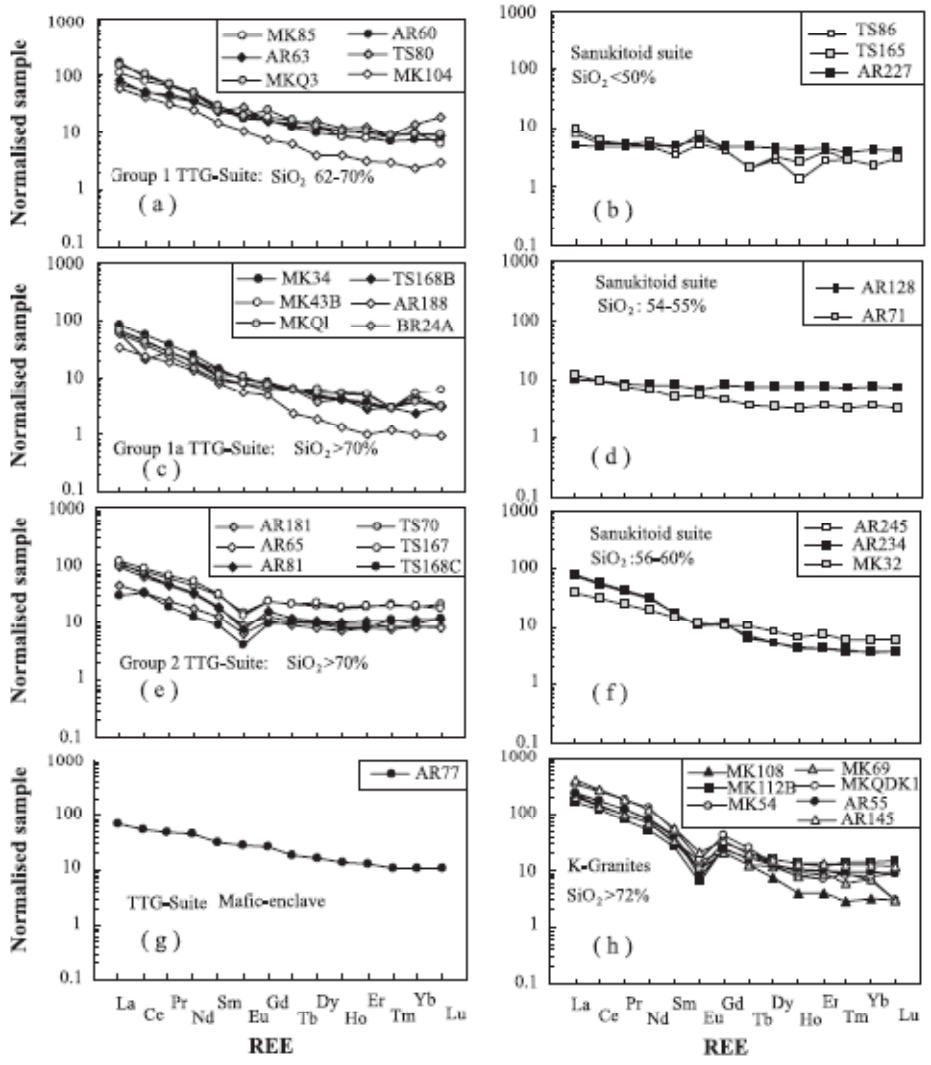

Fig. 10. Representative chondrite-normalised REE patterns for intrusive rocks from the Tati granite–greenstone terrane. Normalising values of Sun and McDonough (1989).

1995). Sr/Y values are variable in the Sanukitoid suite, ranging between ~ 18 and 50 in mafic rocks and 7 and 42 in high-Mg diorites. Sr/Ce ratios are also variable but high in gabbros (36–67) and low to high in Mg diorites (~ 5–22). For comparison, Sr/Ce is ~ 10 in MORB and OIB. Lower values (average ~ 6)

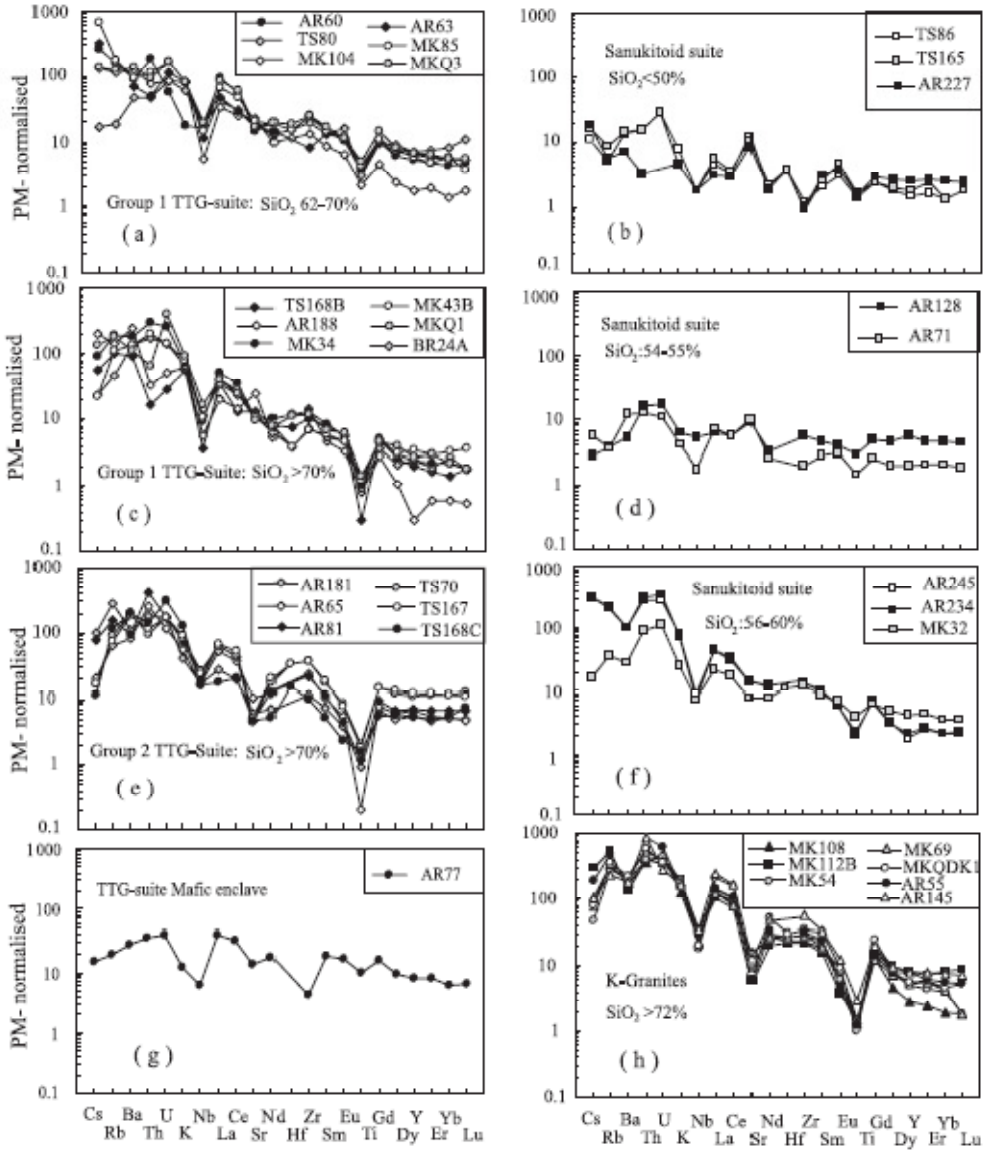

Fig. 11. Representative primordial mantle (PM)-normalised multi-element diagrams for intrusive rocks from the Tati granite–greenstone terrane. Normalising values of Sun and McDonough (1989).

mark sedimentary rocks (e.g. Plank and Langmuir, 1998).

The REE patterns of igneous rocks of the Sanukitoid suite are displayed in Fig. 10b, d and f. Rocks with $SiO_2 < 50\%$ (Fig. 10b) are characterized by flat REE patterns, with $La_N/Yb_N \sim 1-3$, $La_N/Sm_N \sim 1-2$ and $Gd_N/Yb_N \sim 1-2$. Small to moderate Eu positive anomalies ($Eu/Eu^* = 1.3-1.9$) occur in these mafic rocks (Fig. 10b). Intermediate rocks with SiO_2 between 54% and 55% (Fig. 10d) show flat to slightly fractionated REE patterns ($La_N/Yb_N \sim 1-4$, $La_N/Sm_N = 1-3$ and $Gd_N/Yb_N \sim 1$) and very small negative and positive anomalies of Eu ($Eu/Eu^* = 0.8-1.2$). High-Mg diorites with higher SiO_2 content (56–60%) show more fractionated REE patterns (Fig. 10f) marked by higher $La_N/Yb_N = 6-22$, $La_N/Sm_N = 3-4$, $Gd_N/Yb_N = 2-3$ and a moderate Eu negative anomaly in several samples ($Eu/Eu^* \sim 0.7$). The REE pattern features change with the increase of SiO_2 content in the Sanukitoid suite. This change correlates with the increase of incompatible element abundances reported above but does not correlate with a decrease of transition metal abundance.

Primordial mantle normalized spidergrams of Sanukitoid suite rocks are characterized by negative anomalies for Ti, Nb (Ta) and positive anomalies for U and Th (Fig. 11b, d and f). Rocks with $SiO_2 \leq 55\%$ display in addition a Sr positive anomaly and a small Zr negative anomaly (Fig. 11b and d).

5.3. High-K granites

The silica-rich high-K granites (Fig. 3b and c) are characterized by Al_2O_3 contents in the range ~ 12.5–14.5%, Na_2O of ~ 2.5–4.5%, K_2O in the range ~ 3.4–7.9% and $0.9 < A/CNK < 1.1$ (average $A/CNK = 0.99$). These granites are predominantly metaluminous (Fig. 5), with a few slightly peraluminous rocks ($A/CNK > 1$, up to 1.09). These features along with the absence of mineral phases marking strong peraluminous compositions (e.g. cordierite, primary muscovite) suggest that these are I-type granites. The range of transition metal concentrations (Table 1) in the high-K granites and Na-granites of the TTG suite are similar.

The abundances of other trace elements such as alkali, alkali-earth, HFSE and REE are variable, from values similar to those reported in TTG suite rocks of similar SiO_2 content to lower concentrations. A negative anomaly of Eu in chondrite-normalised patterns (Fig. 10h) and negative anomalies for Sr and Ba in primordial-mantle normalised spidergrams (Fig. 11h) mark high-K granites. The incompatible element content of high-K granites and TTG suite rocks show a number of similarities. The high-K granites are marked by a large variation of LREE content (e.g. $La_N \sim 8-397$) but, like TTG suite rocks, show variably fractionated REE patterns ($La_N/Sm_N = 2-7$, $Gd_N/Yb_N = 0.9-6$ and $La_N/Yb_N = 2-66$) and a significantly variable Eu anomaly ($Eu/Eu^* = 0.3-4$). The samples with positive Eu anomalies (Eu/Eu* up to 4) correspond to granite samples affected by hydrothermal alteration (not plotted in Fig. 10 and 11).

The primordial mantle-normalized diagrams (Fig. 11h) show that, at similar SiO_2 content, the high-K granites have higher contents of most incompatible elements (except HREE) than TTG suite rocks. However, the general shape of the spidergrams is similar and both high-K granites (Fig. 11h) and TTG suite rocks (Fig. 11e) are characterized by negative anomalies for Ti, Sr, Nb and Ba in primordial mantle-normalized diagrams.

6. Discussion

6.1. General observations

TTG suite rocks are abundant in the Kaapvaal and Zimbabwe cratons and in the Limpopo belt in southern Africa (e.g. de Wit et al., 1992; Luais and Hawkesworth, 1994; Berger et al., 1995; Berger and Rollinson, 1997).

The Francistown TTG suite defines two distinct petrological groups. The Group 2 TTG sub-suite shows flat chrondrite-normalized HREE patterns and negative Eu anomalies (Fig. 10e) and relatively low Sr/Y ratios (Fig. 9a) indicating its affinities with arc magmas. The geochemical diagrams, e.g. K_2O-Na_2O-CaO (Fig. 3b) and La_N/Yb_N vs. Yb_N (Fig. 9b) show the analogies of the Francistown Group 2 TTG sub-suite rocks with the Cretaceous plutonic rocks from the Peninsular Range and Idaho in USA (e.g. Baird and Miesh, 1984; Gromet and Silver, 1987). These analogies were previously reported by Luais and Hawkesworth (1994) for similar TTG suites

exposed in the centre of the Zimbabwe craton, ~ 300 km NE of the Francistown igneous complex. Group 1 TTG sub-suite rocks display fractionation of both LREE and HREE and no significant negative Eu anomaly in the chondrite-normalized diagrams (Fig. 10c) and are characterised by high Sr/Y ratios (Fig. 9a) marking strongly sodic Archaean TTG suites (Martin, 1993, 1994).

In this paper, Sanukitoid suite rocks are documented for the first time in the Archaean of northeastern Botswana. Jelsma et al. (2001) (and references therein) were the first to describe Neoarchaean high-Mg intermediate rocks from Zimbabwe as Sanukitoids, although the first analyses of high-Mg andesites exposed in the Zimbabwe craton were published by Condie and Harrison (1976). The Sanukitoids provide a strong indication of the overall similarity of the Francistown Neoarchaean plutonic rocks from the Zimbabwe craton to modern volcanic arc magmatism (Tatsumi and Ishizaka, 1982; Shirey and Hanson, 1984; Stern et al., 1989; Stern and Hanson, 1991). The Francistown high-K granitoids display also several petrological analogies with calc-alkaline potassic granites from Phanerozoic orogenic provinces (e.g. Gromet and Silver, 1987; Pitcher, 1993). There are strong chemical similarities between the various granitoids exposed in the Francistown area (Fig. 11), despite some differences marking distinct petrogenetic processes. Petrogenetic models for these rocks must account for their systematic arc-like signature shown by high Al_2O_3, La/Nb, Th/Ta, low TiO_2 and Ce/Pb (in mafic-intermediate rocks) and negative anomalies of Nb–Ti in the primordial mantle normalized diagrams. These features indicate that these igneous rocks formed along a destructive plate margin or were derived largerly from a crustal source that in itself was formed within an arc setting.

In the following section, we discuss in more details our data for the Francistown Neoarchaean plutonic suites in order to constrain the petrogenesis of the rocks and the tectonic setting evolution.

6.2. TTG suite

There is an agreement to consider that the geochemical features of TTG magmas originate from partial melting of a mafic precursor. However, there is a divergence of opinion on the processes involved during the petrogenesis of TTGs. Drummond and Defant (1990) attribute their genesis to partial melting of mafic rocks within a subducting oceanic slab. Alternatively, Petford and Atherton (1996) suggested that TTG magmas form during partial melting of mafic rocks underplated within the crust. Geochemical data do not allow direct discrimination of these two processes. However, melting at the base of (or within) the crust requires the conversion of underplated mafic rocks into garnet amphibolite/eclogite prior to partial melting. The first interpretation requires a tectonically overthickened crust or a steep geothermal gradient beneath the Zimbabwe craton. Tomographic data indicate that the crustal thickness of the Zimbabwe craton is ~ 34–37 km (Nguuri et al., 2001) and exposed rocks are mainly low-gradle (greenschist facies) metamorphic rocks. Therefore this crust has never been overthickened. The second interpretation requires a source of heat to create the steep geothermal gradient. In arc settings, a mechanism that can supply heat for crustal melting is underplating of mafic/ultramafic arc magmas into the lower crust (e.g. Hyndman and Foster, 1988). However, there is not yet evidence to support or reject a linkage between the emplacement of mafic/ultramafic magmas in the crust (magma underplating) and the generation and ascent of the Francistown TTG rocks. The low concentrations of Y, the strong depletion of HREE in the chondrite-normalized diagram (Fig. 10a and c), the absence of Sr negative anomaly in the primordial mantle normalized diagram (Fig. 11c), the overall high concentration of Sr in Group 1 TTG sub-suite rocks and the strong Nb negative anomalies require the presence of garnet and amphibole and no plagioclase in the melt residue. Rushmer (1991) pointed out that amphibole is a stable phase up to 18 kb at 950 °C and therefore it could be among residual minerals during dehydration melting of the oceanic crust. Experimental studies (e.g. Rapp et al., 1991) showed that, during dehydration melting of mafic rocks at ~ 700–1000 °C, the trondhjemitic melt generated has Al-rich composition and the melt residue is plagioclace-free and rich in amphibole and garnet only at high pressure (≥ 1.5 GPa). At lower pressure, the generated melt has calc-alkaline affinity and its composition evolves from Al-poor trondhjemites to diorites/granodiorites, i.e. a magma similar to Group 2 TTG sub-suite rocks in the Tati granite–

greenstone terrane. Plagioclase is stable and therefore its presence in the melt residue could explain the Eu negative anomaly in the Group 2 TTG sub-suite (Fig. 10e). However, it is unlikely that the Group 2 TTG sub-suite was generated under low pressure (<8 kb) since melts generated by both water-undersaturated and water-saturated experiments at such pressures are granodioritic to tonalitic (Helz, 1976) and/or strongly peraluminous (e.g. Holloway and Burnham, 1972; Beard and Lofgren, 1991). In contrast, the Group 2 TTG sub-suite rocks are predominantly metaluminous to slightly peraluminous. Their chemical composition is similar to that of experimental melts produced from garnet amphibolite at pressures between 8 and 15 kb (Rapp, 1997; Wyllie et al., 1997). These data indicate that partial melting of mafic igneous rocks underplated in the lower crust is the most likely source for Group 2 TTG sub-suite rocks in the Tati granite–greenstone terrane.

Numerical models (Peacock et al., 1994) indicated that water-undersaturated (~ 5% H_2O) partial melting of mafic rocks produces a plagioclase-free residual assemblage containing garnet + amphibole. A water-absent melting produces a plagioclase-bearing residue containing two pyroxenes. Thus, the compositional differences between Francistown Groups 1 and 2 TTG rocks could reflect partial melting under different water pressure, i.e. water-absent conditions for Group 2 and water-undersatured conditions for Group 1. The geochemical characteristics require a subduction process during or before the generation of both TTG rocks. In a subduction setting, Group 1 high-Al TTG magmas could originate from partial melting of young, hot, flat subducting oceanic slab with amphibole and garnet as residual phases (e.g. McCulloh, 1993). Sajona et al. (1993) pointed out that melting of old oceanic crust is also possible during the early stages of subduction and/or during fast or oblique subduction. At the regional scale, the Group 1 TTG sub-suite (Grey gneisses) was emplaced early as shown by similar U–Pb SHRIMP ages for TTG rocks and greenstone belt in the Vumba area (Bagai et al., 2002). Preliminary data related to Zimbabwe show a similar relation between ~ 2.7 Ga Neoarchaean TTG and greenstone belts (Jelsma, personal communication, 2000). Therefore, the Neoarchaean high-Al TTG sub-suite in the Zimbabwe craton most probably indicate partial melting of a flat subducting slab as documented in modern settings (e.g. Gutscher et al., 2000).

6.3. Sanukitoid suite

Sanukitoids and Sanukitoid-like igneous suites occur in both Archaean and post-Archaean igneous provinces. The high Mg# and relatively high transition metal contents (Table 1) suggest an ultramafic mantle source for the primary magmas of the Francistown Sanukitoid suite. The high-Mg diorites display a number of geochemical features indicating their affinity with modern arc igneous rocks. These include high values for Th/Ta, La/Nb, Cs/La, Ba/Th, Ba/La and negative Ti–Nb (Ta) anomalies in primordial mantle normalized diagrams (Fig. 11). The gabbros show most of the above features but their Th/Ta and La/Nb ratios are close to values marking extensional mafic igneous rocks. Both Sanukitoid gabbros and Mg-diorites are enriched (Figs. 10 and 11), with the strongest REE enrichment occurring in the Mg-diorites containing >55% SiO_2 and marked by the highest Ni concentrations (Table 1). As stated before, the Mg-diorites were not formed by mafic mineral fractionation from gabbroic magmas since they usually have similar or higher Mg# and transition metal concentrations. Although small degree of partial melting of a sub-arc mantle could produce an enrichment in incompatible trace elements (e.g. LILE and HFSE), it cannot explain the extremely high and variable ratios between incompatible elements such as the LILE/HFSE ratios (e.g. Th/Ta and La/Nb) reported above. The geochemical characteristics suggest that the Sanukitoid gabbros and Mg-diorites originate from an heterogenous mantle source.

The elemental compositions and inter-element ratios reported above are similar to values documented in arc igneous provinces and linked to three main processes: (1) mantle wedge enrichment by sediments recycled in the mantle along subducting slabs (e.g. Plank and Langmuir, 1993); (2) mantle wedge enrichment by fluids from the dehydration of a subducting slab (e.g. Keppler, 1996; Tatsumi and Kogiso, 1997); (3) enrichment of the sub-arc mantle by slab-derived melts (e.g. Kelemen, 1995; Yogodzinski et al., 1995; Kepezhinskas et al., 1996; Sajona et al., 2000). The studies related to the mobility of elements in the aqueous fluids escaping from the subducting slab

(e.g. Stolper and Newman, 1994; You et al., 1996) showed that more than 95% by mass are made of LILE and other highly incompatible elements. LREE have low to moderate mobility whereas HREE are the least mobile. Therefore, arc magmas derived from partial melting of a mantle wedge enriched by fluids escaping from a subducting slab will be characterized by a strong enrichment in LILE (e.g. Sr, Pb and Hf) versus a moderate enrichment in LREE, leading to high LILE/LREE in the melt. Mafic magmas generated in a sub-arc mantle source enriched by slab-derived fluids are generally marked by high Sr/Ce values ($\gg$20), low Sr/Y ratios (Fig. 9a) and low Ce/Pb ratios ($\ll$20) (e.g. Chauvel et al., 1995; Kapenda et al., 1998). However, Sajona et al. (2000) stressed that the same enrichment style characterizes mantle wedge sections metasomatized by slab melts. In contrast, mafic magmas originating from a sub-arc mantle enriched by subducting sediment melts are marked by low Sr/Ce, Ce/Pb and Sr/Y values. Shimoda et al. (1998) suggested that subducting sediment melts represent the main mantle wedge enrichment agent at the source of Setouchi Mg-andesites. However, this interpretation is unlikely for the Francistown Sanukitoid gabbros and high-Mg diorites marked by high to very high Sr/Ce ratios and high Sr/Y values (Fig. 9a). Mg-diorites with low values of Sr/Y and Sr/Ce (e.g. down to 5) could, however, originate from a mantle source enriched by sediments melts. The increase of silica correlated to an increase of LREE and fractionation of HREE in the Francistown Sanukitoid suite indicates a mantle source enrichment predominantly controlled by a silicate melt. The strong fractionation of LREE in high-Mg diorites suggest melting under high pressure, within the stability field of garnet, whereas the strong fractionation of HREE indicates partial melting of an enriched mantle wedge. Both features could originate from partial melting of a mantle wedge that was enriched by silicate melts formed within the stability field of garnet. The negative Nb anomaly suggests the presence of amphibole in the melt residue. The high K_2O content of high-Mg diorites requires a K-rich mineral phase(s) at the source, most probably phlogopite and/or K-amphibole. However, K_2O contents are not high in all the rocks of this suite. This indicates that the distribution of the K-rich mineral phase(s) in the melt source was heterogeneous. The heterogeneity of the mantle source is also indicated by the large variation of ratios between incompatible trace elements, e.g. Th/Ta, Nb/Ta, La/Nb, Sr/Ce, etc. The coexistence of enriched rocks with both flat (Fig. 10b and d) and fractionated (Fig. 10f) REE patterns support this interpretation. In addition to SiO_2, Na_2O/K_2O and Sr/Y ratios are high in the Sanukitoid rocks, including in K_2O-rich high-Mg diorites. These features indicate that the mantle source metasomatizing agent was a silica- and Na-rich melt, pointing towards a sub-arc mantle enrichment controlled by Al-rich (Group 1) TTG melts, which were emplaced before the Sanukitoids in the Francistown region. Schiano et al. (1995) documented mantle xenoliths from arc settings containing hydrous silica-rich melt inclusions of high-Mg andesitic composition in olivine grains. This observation supports the mantle origin of Mg dioritic magmas. Experimental studies (e.g. Sen and Dunn, 1995; Rapp et al., 1999) showed that the interaction between silica-rich melts and peridotites produces metasomatic ultramafic rocks containing garnet, amphibole, phlogopite and two pyroxenes. Partial melting of a metasomatized mantle with such a paragenesis would be an appropriate source for the Francistown Sanukitoid rock suite.

Yogodzinski et al. (1995) suggested that Archaean Sanukitoids could originate from direct partial melting of subducted mafic oceanic crust. This could explain several geochemical features of the Francistown Sanukitoids such as Ce/Pb, Sr/Y, Th/Ta, La/Nb, Cs/La, Ba/Th and Ba/La ratios and Ce negative anomaly documented in a few rock samples (e.g. TS 168B; Fig. 10c). Cerium negative anomaly is known to occur in oceanic mafic rocks affected by seawater alteration (e.g. Hole et al., 1984). It has also been documented in fresh arc mafic rocks where it is inherited from the mantle source enriched by fluids or melts from an oceanic crust affected by seawater alteration (e.g. Hole et al., 1984; Elliot et al., 1997). However, the Francistown Sanukitoid rocks are not the product of direct partial melting of a subducting slab because they are characterized by high Mg# and high concentration of transition metals in high-Mg diorites.

A number of workers (e.g. Stern and Hanson, 1991; Stevenson et al., 1999) stressed the geochemical similarities between Sanukitoids and calc-alkaline magmas and suggested the derivation of Sanukitoids

from partial melting of a sub-arc peridotitic mantle wedge enriched by fluids expelled from a subducting slab. Although this interpretation can explain a number of geochemical characteristics of the Francistown Sanukitoids, it cannot explain the high SiO_2, Ni and Cr contents, low Sr/Ce ratios of some high-Mg diorites and high Sr/Y values of mafic rocks of the Francistown Sanukitoid suite. In addition, it is not consistent with the low Mg# and transition metal abundances marking experimental melts from amphibolite or eclogite (Rapp et al., 1991; Sen and Dunn, 1994). Kelemen et al. (1993) pointed out that high Mg# and transition metal contents of high-Mg andesites are acquired during interaction of silica-rich slab-derived melt with the overlying mantle and this is consistent with the following geochemical features of the Francistown Sanukitoid suite: (1) an increase of SiO_2 from gabbros to Mg-diorites and a correlative increase of LREE shown by an increase of La_N/Sm_N and La_N/Yb_N; (2) a substantial LREE and HREE fractionation in the high-Mg diorites (Fig. 10f) and no REE fractionation in the mafic rocks (Fig. 10b); (3) high Ni and Cr abundances requiring an ultramafic source. Altogether, the geochemical data indicate that the source of the Sanukitoid suite is a sub-arc mantle wedge variably metasomatized by both TTG melts and fluids escaping from the subducting slab. The high-Mg diorites originate from a mantle section strongly metasomatized during the ascent of earlier TTG melts. High pressure experimental investigations by Rapp et al. (1999) showed that slab-derived silica-rich melt interacting with mantle peridotite during ascent becomes Mg-rich but preserves its main geochemical features, e.g. high SiO_2 content, high LREE enrichment, fractionation of REE and high Sr/Y ratios. In addition, the ascending silicate melt is used in reactions converting the mantle peridotite assemblages into a metasomatic assemblage made of garnet-phlogopite-amphibole-two pyroxenes, a paragenesis inferred above for the source of the Francistown Sanukitoids and documented in mantle xenoliths from arc settings (e.g. Vidal et al., 1989).

6.4. High-K granites

Two main models can account for the genesis of granites: (1) fractional crystallisation of a mantle-originating mafic magma, combined or not with crustal assimilation; (2) partial melting of crustal rocks. The Francistown high-K granites are part of a large late to post-orogenic potassic granite province known as the Chilimanzi granite suite in the Zimbabwe craton. There is no evidence suggesting a linkage of this large potassic granitic province to mantle-originating mafic magmas, although these granitoids are partly coeval to the emplacement of the Great Dyke in Zimbabwe (e.g. Armstrong and Wilson, 2000). The high SiO_2 contents of these granites preclude a direct mantle origin.

The Francistown high-K granites are metaluminous to slightly peraluminous (Fig. 5) and show affinities to I-type potassic calc-alkaline granites. Their chondrite normalized REE patterns are similar to those of calc-alkaline felsic rocks from modern continental active margins, e.g. rhyolites and granites from the Cascades in California, USA (e.g. Tepper et al., 1993; Borg and Clynne, 1998). However, similar rocks are also emplaced during late-to post-orogenic evolution of orogenic belts (e.g. Pitcher, 1993) and they mark late to post-orogenic evolution of most Archaean cratons (e.g. Tchameni et al., 2000).

In California, high-K felsic rocks chemically similar to the Francistown high-K granites were attributed to large proportions (~ 35–45%) of partial melting of a mafic lower crust. Dehydration melting experiments of mafic rocks between ~ 800 and 1100 °C yielded felsic melts with calc-alkaline composition (e.g. Beard and Lofgren, 1991; Rushmer, 1991; Wolf and Wyllie, 1994; Patiño Douce and Beard, 1995). The negative Eu anomaly in the REE patterns (Fig. 10) suggests substantial plagioclase in the residual assemblage and, according to Tepper et al. (1993), this would indicate melting under low a_{H_2O}. The flat HREE patterns of some high-K granites (e.g. $0.9 < Gd_N/Yb_N < 1.9$ in samples MK112A, B, MKQ 5 and MK 31B) and their relatively high Y and Yb contents indicate a garnet-free source. Although host–rock composition dependent, garnet is generally absent in dehydration melting experiments conducted at < 8 kb (Rushmer, 1991; Rapp et al., 1991), whereas it is present in similar experiments at ~ 10 kb (Wolf and Wyllie, 1994). Therefore, the Francistown high-K granites have most probably been generated at pressures < 8 kb, i.e. within the middle or the lower crust as already proposed above. To reach the critical melt fraction of ~ 30–40% required for felsic melt to separate from

its source and define discrete magma bodies (Wickham, 1987), we infer that temperatures in excess of 900 °C were required.

The composition of the source rocks can be inferred from the chemical composition of the granites. Roberts and Clemens (1993) pointed out that, because of their low K_2O contents, metabasaltic rocks are unsuitable sources for high-K, I-type granitoids. According to these authors, these granites are derived from partial melting of metamorphosed hydrous intermediate calc-alkaline rocks. Experimental data of Carrol and Wyllie (1989) indicate that partial melting of tonalites could produce high-K granite melts and thus we infer that TTG material represents the potential source rocks for the high-K granites in the Zimbabwe craton. The Francistown high-K granites show a large variation of composition in terms of LILE and REE (Figs. 10 and 11). However, this suite includes rocks having the highest incompatible element contents in the Francistown granitoids. The overall shape of the Francistown high-K granites in primordial mantle normalized diagrams (Fig. 11) are identical to the patterns of the TTG suite rocks (Fig. 11c and e). Thus, the high-K granites most probably formed by partial melting of TTG rocks. Particularly, the granites with flat HREE patterns (e.g. $La_N/Yb_N \sim 0.94$ in sample MK 31B) most probably were formed by partial melting of Group 2-like TTG rocks. The high-K granite MK 108 shows a fractionated HREE pattern (Fig. 11h), with $La_N/Yb_N \sim 6.4$ suggesting that it could originate from Group 1-like TTG sub-suite rocks. Melting of a source including both Groups 1 and 2 TTG sub-suite rocks could produce melts with geochemical features intermediate between these two end-member source rocks. Our interpretation is in line with the results of previous workers (e.g. Luais and Hawkesworth, 1994) who showed that, in the Zimbabwe craton, the youngest granitoids originate from partial melting, within the crust, of earlier TTG material.

6.5. Tectonic implications

The geochemical data indicate that the Neoarchaean Francistown granitoids are marked by: (1) a high-Al (Group 1) TTG sub-suite originating from partial melting of a subducting slab; (2) a low-Al (Group 2) TTG sub-suite originating from partial melting of arc mafic igneous rocks underplated and metamorphosed in the lower crust; (3) a Sanukitoid suite ultimately derived from a sub-arc mantle wedge enriched by silica-rich TTG melts and fluids escaping from a subducting slab; and (4) younger crustally derived high-K granites resulting from partial melting of TTG material. Treloar et al. (1992) suggested the genesis of these high-K granites could indicate a major crustal thickening following continental collision. However, there are no S-type granites in the Francistown region and in the rest of the Zimbabwe craton despite the presence of supracrustal sedimentary rocks and low-grade metasedimentary assemblages. Thus, there was no major tectonically induced overthickening of the crust beneath the Zimbabwe craton and this is compatible with geophysical data indicating a crustal thickness between 34 and 37 km (Nguuri et al., 2001). The layer-parallel shear zones and thrusts active between ~ 2.68 and 2.6 Ga in the Zimbabwe craton (e.g. Kusky and Kidd, 1992; Dirks and Van der Merwe, 1997; Jelsma and Dirks, 2000; Bagai et al., 2002; Dirks et al., 2002) induced a limited thickening of the crust, probably similar to tectonic thickening in modern accretionary orogens (e.g. Andes). Dirks et al. (2002) suggested that these layer-parallel shear zones and thrusts formed during a shallow subduction process or underplating. Geochemical data in this paper support a flat slab model.

High-K granites are widespread in the Zimbabwe craton whereas coeval mafic rocks are only developed along the Great Dyke (e.g. Armstrong and Wilson, 2000). The absence of large volume of mafic rocks spatially closely related to the high-K granites implies that mafic magma underplating is probably not the source of heat responsible for the generation of the granites. The alternative process allowing to heat the lower crust is the juxtaposition of the asthenospheric mantle against the base of the crust. This could happen during delamination (detachment) of a subducting slab (e.g. Houseman et al., 1981) and does not require Himalayan-type continental collision.

The magmatic suites identified in the Francistown igneous province define a consistent tectono-magmatic evolution pattern marked by the following:

(1) A shallow-dipping (flat) subduction during the earliest stage leading to partial melting of the subducting slab to produce the high-Al TTG sub-suite (Group 1). The earliest ductile fabric reported in the

Francistown TTG rocks and unknown in the adjacent (younger) Sanukitoid rocks mark a shortening event during this earliest igneous event and this is compatible with a flat subduction. During flat subduction, there is a higher interplate coupling and the cold, strong rheology of the overriding lithosphere enables stress and deformation to be transmitted far inboard into the upper plate (e.g. Pubellier and Cobbold, 1996). Shallow-dipping subduction systems are marked by wide arc systems, extending much further ($\geq$ 400 km) from the trench (Gutscher et al., 2000). In the case of central Chile, Kay and Abbruzzi (1996) indicated that the arc above the central Andean flat slab extends between 250 and 800 km from the trench. This could explain the large area covered by Neoarchaean TTG rocks and affected by ca. 2.7–2.6 Ga layer-parallel shear zones and thrusts in the Zimbabwe craton.

(2) Generation of the Sanukitoid suite by partial melting of a sub-arc mantle wedge enriched during the ascent of the earlier TTG melts. The absence of TTG igneous rocks emplaced at the same time or mixed with the Sanukitoid suite rocks suggest that the partial melting of the subducting slab had ceased when the Sanukitoid magmas were produced. We speculate that the transition from TTG to Sanukitoids could correspond to a change from shallow to a steep subduction. It is known that flat subduction alters the thermal structure of an active margin because of the insertion of cold oceanic lithosphere beneath the upper lithosphere in the area where normally hot asthenosphere occurs in the case of steep subduction (e.g. Davies, 1999). Therefore, prolonged flat subduction cools both plates and increases the strength of the upper plate (Vlaar, 1983; Spencer, 1994). We infer that a substantial cooling of the downgoing slab beneath the Zimbabwe craton shut its melting and favoured the conversion of basaltic rocks into eclogites, leading to a steeper subduction regime and related partial melting of the sub-arc mantle wedge (cf. Sanukitoid suite). An important observation from our geochemical data is that the ratios Cs/La, Ba/Th, Ba/La point to the emplacement of the Francistown Sanukitoids at or close (<50 km) to the volcanic arc front. This requires a trench, which was relatively close to Francistown during the Neoarchaean and, as there is no evidence of extreme crustal overthickening in the region, presumably the trench sediment infill should still be preserved in the vicinity. In our interpretation, the supracrustal (meta) sedimentary rocks exposed in the Shashe belt represent remnants of the Neoarchaean accretionary sedimentary packages. The Matsitama greenstone belt, which is close to this inferred trench sedimentary package, contains mafic rocks with geochemical affinities with oceanic arc tholeiites (Majaule et al., 1997). Geophysical studies have shown that the Shashe belt is the western extension of the Neoarchaean Limpopo belt (Ranganai et al., 2002). Therefore, the subduction along the Limpopo–Shashe belt presumably controlled the genesis and emplacement of the 2.7–2.6 TTG and Sanukitoid suites in the Zimbabwe craton. This implies a northerly-dipping subduction zone, and this is in agreement with the north–south Neoarchaean shortening documented in the southern part of the Zimbabwe craton by Treloar and Blenkinsop (1995). Granitoids exposed in the Limpopo–Shashe belt are coeval to the TTG suite in the Zimbabwe craton (Majaule and Davis, 1998; Kröner et al., 1999). The convex-shape of the Limpopo–Shashe belt compares to the shape of the Pacific subduction system along the Aleutian trench in Alaska (North America) or the Makran plate convergence zone between the Arabian and Iranian microplates, and is most probably a primary feature. A convex subduction along the Limpopo–Shashe belt implies, in present day coordinates, a west to northwest-dipping subduction zone to the east of the Zimbabwe craton and a northeast-dipping subduction zone to the west of the craton. In such a continental active margin, the layer-parallel shear zones and thrust developing in the overriding plate will be marked by cratonward transport direction, i.e. towards the northeast in the west of the craton and westward/northwestward in the east. This is compatible with available structural data (Dirks and Van der Merwe, 1997; Jelsma and Dirks, 2000; Dirks et al., 2002; Paya and Kampunzu, unpublished data).

Several authors (e.g. Cloos, 1993; Gutscher et al., 2000 and references therein) indicated that flat subduction are common where ridge or oceanic plateaus are subducting. The Central Zone of the Limpopo belt includes mafic–ultramafic rocks chemically similar to mafic rocks along the Chile-type oceanic ridge and emplaced when this ridge was subducting beneath southern America (Kampunzu et al., 2002, this volume). The subduction and partial melting of this type

of oceanic basalts would provide an adequate source for the high-Al TTG sub-suite in the Zimbabwe craton. Seismic tomography investigations showed that slab melting is closely linked to flat subduction of thick oceanic crust (e.g. Gutscher et al., 2000). Therefore, the Francistown TTG probably reflects a flat subduction of a thick oceanic crust, i.e. an oceanic plateau or an arc. Presumably, this process was common during the Archaean, leading to frequent slab melting (e.g. Martin, 1993, 1994). It is known that both the overriding plate and the subducting slab are cooled by flat subduction (e.g. Vlaar, 1983; Spencer, 1994). Cooling the subducting lithosphere delays the basalt to eclogite transition but once this happens, the average density of the downgoing slab would increase and this should induce a change from flat to steeper subduction (e.g. Abbott et al., 1994). The production of TTG magmas will cease with that change. A steep subduction favours dehydration of fluids from the subducting-slab which enrich the mantle wedge leading to the generation of calc-alkaline mafic magmas (e.g. Pearce, 1982). The Francistown Sanukitoid suite rocks have geochemical affinities with calc-alkaline magmas and this probably indicate a fluid input at the mantle source but bear also the geochemical imprint of a sub-arc mantle metasomatism induced by the ascent of earlier TTG melts.

Condie and Harrison (1976) reported "tholeiitic" mafic rocks in the Zimbabwe craton (between ~ 18–20°S and 29–30°E). These rocks show chemical similarities with the Francistown Sanukitoid suite mafic rocks. In addition, the andesites reported by these authors in the same area contain on average ~ 6% MgO at ~ 57% SiO_2 and corresponds to Mg-andesites similar to the Sanukitoid Mg-diorites documented in this paper. According to Jelsma (personal communication, 2002), the Nd and Pb isotopic compositions published by Jelsma et al. (1996) relate to the Sanukitoid rocks in Zimbabwe. They show positive (+2 to +3) epsilon Nd_T and identical U–Pb zircon and T_{DM} model ages at ca. ~ 2.64 Ga. These data point to mantle origin for the Sanukitoids as proposed in this study. The high-μ value reported by Jelsma et al. (1996) for the source of these rocks support the subduction model proposed during the genesis of the Francistown Sanukitoids. The areal coverage of the Sanukitoid volcanism in the Zimbabwe craton is yet not known but conservative estimate using the data from this study and from Condie and Harrison (1976) is >1000 km^2. It indicates an important continental active margin and probably a steeper subduction process in the evolution of the Limpopo–Shashe accretionary system. Our interpretation is close to that of Berger and Rollinson (1997) who pointed out that Neoarchaean crustal growth within the Northern Marginal Zone of the Limpopo belt in Southern Zimbabwe compares with modern continental convergent margins such as the Andes (see also Berger et al., 1995). We further contend that the Neoarchaean magmatism at ~ 2.8–2.6 Ga in the Zimbabwe craton and the Limpopo–Shashe belt are linked to various evolutionary stages of a single Andes-type long-lived active continental margin, with an earlier flat subduction stage (generation of high-Al TTGs) relayed by a steeper subduction (emplacement of Sanukitoids). The seismic tomography map of the Zimbabwe craton (James et al., 2001) shows a fast mantle and a keel beneath the Zimbabwe craton. We infer that this mantle root represents the residual mantle wedge after extraction of the arc magmas.

Previous geodynamic models assuming that the ~ 2.8–2.5 Ga magmatism in the Zimbabwe craton was emplaced in a classical continental rift setting (e.g. Nisbet et al., 1981; Blenkinsop et al., 1993; Jelsma et al., 1996) are not supported by our data. Hunter et al. (1998) linked the ~ 2.7 Ga Belingwe greenstone belt (Zimbabwe) to an extensional (rift) setting based on sedimentological data (e.g. proximal thin sedimentary deposits, heterogeneity of the sedimentary rocks indicating very local sources) and the presence of komatiites inferred to mark a plume. However, the above sedimentological features could as well be accommodated in a steep subduction model known to be characterised by the development of extensional basins in the upper plate. In addition, komatiites can form in arc settings (T. Grove, personal communication, 2000; see also Parman et al., 1997), although there is no agreement on this question (Herzberg and O'Hara, 1998 and references therein).

Kusky (1998) proposed that the Tati and Vumba greenstone–granite terranes represent an oceanic plateau accreted onto the Zimbabwe craton and subsequently affected by arc magmatism. Geochemical data (Bagai, 2000; this paper and our unpublished data) do not support this interpretation. The

Vumba and Tati greenstone belts and related granitoids are part of arc magmatism; there is no evidence for an oceanic plateau in these two greenstone belts.

The Francistown high-K granites and correlative granitoids of the Chilimanzi suite in Zimbabwe have structural features (e.g. Mkweli et al., 1995; Frei et al., 1999) and geochemical characteristics (this paper) which are compatible with their genesis in a late to post-orogenic environment. There is no evidence of magmatism due to overthickening of continental crust in the Zimbabwe craton. S-type plutons, which would be significant in such a setting, are absent and the I-type composition of the voluminous late-to post-orogenic high-K granites in the Zimbabwe craton indicates partial melting of TTG bodies underplated in the lower crust. A potential tectonic model for the high-K granites, in line with the geotectonic interpretation of the Francistown Sanukitoid and TTG suites, would be the detachment (delamination) of the subducting slab (e.g. Houseman et al., 1981; Kampunzu et al., 1998). Steepening of the subducting slab most probably led to its detachment, allowing upwelling of a hotter and deeper mantle section supplying heat for crustal melting of earlier TTG material. This interpretation is supported by metamorphic studies indicating a ~ 2.6–2.5 LP-HT granulite facies metamorphism (Berger et al., 1995; Blenkinsop and Frei, 1996; Kamber et al., 1996) showing an anticlockwise P–T–t path in the NMZ (Kamber and Biino, 1995). On this reasoning the main region of delamination lay within and north of the NMZ, consistent with the occurrence of large volumes of Chilimanzi-type granitoid plutons in Zimbabwe.

7. Conclusion

The Neoarchaean (~ 2.7–2.6 Ga) intrusive bodies exposed at the southwestern margin of the Zimbabwe craton in NE Botswana represent three distinct magmatic suites: (1) TTG suite made of tonalites–trondhjemites and Na-granites; (2) Sanukitoid suite including gabbros and Mg-diorites; and (3) high-K granites which are part of the Zimbabwe craton-wide Chilimanzi late- to post-orogenic granitoid suite. These three magmatic suites occur also in the centre of the Zimbabwe craton.

Major and trace element compositions of these three magmatic suites indicate the following features:

(1) High-Na, Sr and Sr/Y, enrichment in LILE and REE, fractionation of both LREE and HREE and no negative Eu anomaly in the chondrite-normalized patterns of Al-rich (Group 1) TTG sub-suite rocks. These features indicate the genesis of these magmas by partial melting of a subducting slab. The Al-poor (Group 2) TTG sub-suite rocks originate from partial melting (8 kb $< P <$ 15 kb) of garnet amphibolites representing underplated arc mafic rocks metamorphosed at the base or within the lower crust;
(2) High-Mg diorites which are rich in transition metals, LILE and LREE and possess steeply fractionated REE profiles. These geochemical features are typical for Archaean Sanukitoids and modern Mg-andesites in arc settings. The transition metal and incompatible trace element contents are high in these silica-rich magmas. The enrichment style (e.g. Nb–Ti negative anomalies, low Ce/Pb, high SiO_2 and transition metal contents, high La/Nb, Th/Ta, Ba/La, Cs/La, Ba/Th) are consistent with a sub-arc enriched mantle source for the Sanukitoid suite. TTG melts from melting of the subducting slab and fluids escaping from the downgoing slab represent the most important metasomatising agents of this mantle source;
(3) High-K granites originate from crustal melting of earlier TTG material. There is no evidence for or against partial melting triggered by underplating of arc mafic magmas to produce these granites.

However, the evolution from TTG to Sanukitoids and to high-K granites is here taken to indicate a progressive change from an earlier flat subduction of a hot lithosphere to a steeper subduction induced by the cooling of the slab during the subduction process and finally a break-off and detachment of this steep slab. This detachment allowed the uprise of hotter mantle material, which supplied the required heat for crustal melting of earlier TTG to produce high-K granites. We believe that the Francistown igneous suites and coeval igneous rocks in the Zimbabwe craton and Limpopo–Shashe belt represent a single accretionary system including: (1) a continental mag-

matic arc within the Zimbabwe craton and (2) an accretionary sedimentary and volcanic/plutonic assemblage within the southward-convex Limpopo–Shashe belt.

Acknowledgements

This is a contribution to the Kaapvaal Craton Project. A.B.K., M.M., M.Z. and Z.B. acknowledge the logistic and financial support of University of Botswana (UB) to the Kaapvaal Craton Project (RPC Grant R#442) and the logistic support of Geological Survey of Botswana (DGS) to the UB Kaapvaal Craton Team. We acknowledge the contribution to this research of Year 4 students from University of Botswana (Segwabe and Keeletsang: academic year 1997/1998; Keitumetse, Ntere and Rachere: academic year 1999/2000). A.R.T. and T.M. acknowledge the DGS for supporting the involvement of their staff into the Kaapvaal Project. This paper is published with the authorisation of the Minister of Mineral, Energy and Water Affairs and of the Director of Geological Survey Department, Botswana.

References

Abbott, D., Drury, R., Smith, W.H.F., 1994. Flat to steep transition in subduction style. Geology 22, 937–940.

Akdiss, D.T., 1991. The Motloutse Complex and the Zimbabwe craton/Limpopo belt transition in Botswana. Precambrian Res. 50, 89–109.

Armstrong, R., Wilson, A.H., 2000. A SHRIMP U–Pb study of zircons from the layered sequence of the Great Dyke, Zimbabwe, a granitoid anatectic dyke. Earth Planet. Sci. Lett. 180, 1–12.

Bagai, Z., 2000. Geochemical and geochronological investigations of the Vumba granite–greenstone terrain of NE Botswana. MPhil Thesis, Univ. Durham, UK. 174 pp.

Bagai, Z., Armstrong, R., Kampunzu, A.B., 2002. U–Pb single zircon geochronology of granitoids in the Vumba granite–greenstone terrain (NE Botswana): implication for the Archaean Zimbabwe craton. Precambrian Res. 118, 149–168.

Baird, A.K., Miesh, A.T., 1984. Batholithic rocks of southern California—a model for the petrological nature of their source material. U.S. Geol. Surv. Prof. Paper, vol. 1284. 42 pp.

Barker, F., 1979. Trondhjemite: definition, environment, and hypotheses of origin. In: Barker, F. (Ed.), Trondhjemites, Dacites and Related Rocks. Elsevier, Amsterdam, pp. 1–12.

Beard, J.S., Lofgren, G.E., 1991. Dehydration melting and water-saturated melting of basaltic and andesitic greenstones and amphibolites at 1, 3 and 6.9 kb. J. Petrol. 32, 465–501.

Berger, M., Rollinson, H., 1997. Isotopic and geochemical evidence for crust–mantle interaction during late Archaean crustal growth. Geochim. Cosmochim. Acta 61, 4809–4829.

Berger, M., Kramers, J.D., Nagler, Th.F., 1995. Geochemistry and geochronology of charnockites and enderbites in the Northern Marginal Zone of the Limpopo belt, Southern Africa, and genetic models. Schweiz. Mineral. Petrogr. Mitt. 75, 17–42.

Bickle, M.J., Nisbet, E.G., Martin, A., 1994. Archaean greenstone belts are not oceanic crust. J. Geol. 102, 121–138.

Blenkinsop, T.G., Frei, R., 1996. Archaean and Proterozoic mineralisation and tectonics at Renco mine (Northern Marginal Zone, Limpopo belt, Zimbabwe). Econ. Geol. 91, 1225–1238.

Blenkinsop, T.G., Fedo, C.M., Bickle, M.J., Eriksson, K.A., Martin, A., Nisbet, E.G., Wilson, J.F., 1993. Ensialic origin for the Ngezi Group, Belingwe greenstone belt, Zimbabwe. Geology 21, 1135–1138.

Blenkinsop, T.G., Martin, A., Jelsma, H.A., Vinyu, M.L., 1997. The Zimbabwe craton. In: de Wit, M.J., Ashwal, L.D. (Eds.), Greenstone Belts. Clarendon Press, New York, pp. 567–580.

Borg, L.E., Clynne, M.A., 1998. The petrogenesis of felsic calc-alkaline magmas from the southernmost Cascades, California: origin by partial melting of basaltic lower crust. J. Petrol. 39, 1197–1222.

Carroll, M.J., Wyllie, P.J., 1989. Experimental phase relations in the system tonalite–peridotite–H_2O at 15 kbar, implications for assimilation and differentiation processes near the crust–mantle boundary. J. Petrol. 30, 1351–1382.

Chauvel, C., Goldstein, S.L., Hofman, A.W., 1995. Hydration and dehydration of oceanic crust controls Pb evolution in the mantle. Chem. Geol. 126, 65–75.

Cloos, M., 1993. Lithospheric buoyancy and collisional orogenesis: subduction of oceanic plateaus, continental margins, island arcs, spreading ridges, and seamounts. Geol. Soc. Am. Bull. 105, 715–737.

Condie, K.C., 1989. Geochemical changes in basalts and andesites across the Archean–Proterozoic boundary: identification and significance. Lithos 23, 1–18.

Condie, K.C., Harrison, N.M., 1976. Geochemistry of the Archean Bulawayan Group, Midlands greenstone belt, Rhodesia. Precambrian Res. 3, 253–271.

Coward, M.P., James, P.R., Wright, L., 1976. Northern margin of the Limpopo orogenic belt, southern Africa. Geol. Soc. Am. Bull. 87, 601–611.

David, K., Schiano, P., Allègre, C.J., 2000. Assessment of the Zr/Hf fractionation in oceanic basalts and continental materials during petrogenetic processes. Earth Planet. Sci. Lett. 178, 285–301.

Davies, J.H., 1999. Simple analytic model for subduction zone thermal structure. Geophys. J. Int. 139, 823–828.

de Wit, J.M., Roering, C., Hart, R.J., Armstrong, R.A., De Ronde, C.E.J., Green, R.W.E., Tredoux, M., Peberdy, E., Hart, R.A., 1992. Formation of an Archaean continent. Nature 357, 553–562.

Dirks, P.H.G.M., Van der Merwe, J., 1997. Early duplexing in an Archaean greenstone sequence and its control on gold mineralization. J. Afr. Earth Sci. 24, 603–620.

Dirks, P.H.G.M., Jelsma, H.A., Hofmann, A., 2002. Thrust-related accretion of an Archaean greenstone belt in the Midlands of Zimbabwe. J. Struct. Geol. 24, 1707–1727.

Dodson, M.H., Williams, I.S., Kramers, J.D., 2001. The Mushandike granite: further evidence for 3.4 Ga magmatism in the Zimbabwe craton. Geol. Mag. 138, 31–38.

Dostal, J., Mueller, W., 1992. Archean shoshonites from the Abitibi greenstone belt, Chibougamau (Quebec, Canada): geochemistry and tectonic setting. J. Volcanol. Geotherm. Res. 53, 145–165.

Drummond, M.S., Defant, M.J., 1990. A model for trondhjemite–tonalite–dacite genesis and crustal growth via slab melting: Archaean to modern comparisons. J. Geophys. Res. 95, 21503–21521.

Elliot, T., Plank, T., Zindler, A., White, W., Bourdon, B., 1997. Element transport from slab to volcanic front at the Mariana arc. J. Geophys. Res. 102, 14991–15019.

Frei, R., Blenkinsop, T.G., Schönberg, R., 1999. Geochronology of the late Archaean Razi and Chilimanzi suites of granites in Zimbabwe: implications for the late Archaean tectonics of the Limpopo belt and Zimbabwe craton. S. Afr. J. Geol. 102, 55–63.

Gill, J.B., 1981. Orogenic Andesites and Plate Tectonics Springer-Verlag, Berlin. 389 pp.

Gromet, L.P., Silver, L.T., 1987. REE variations across the Peninsular Ranges batholith: implications for batholithic petrogenesis and crustal growth in magmatic arcs. J. Petrol. 28, 75–125.

Gutscher, M.A., Maury, R., Eissen, J.P., Bourdon, E., 2000. Can slab melting be caused by flat subduction? Geology 28, 535–538.

Hamilton, W.B., 1998. Archean magmatism and deformation were not products of plate tectonics. Precambrian Res. 91, 143–179.

Helz, R., 1976. Phase relations of basalts in their melting ranges at P_{H_2O}=5 kb: Part 2. Melt compositions. J. Petrol. 17, 139–193.

Herzberg, C., O'Hara, M.J., 1998. Phase equilibrium constraints on the origin of basalts, picrites, and komatiites. Earth Sci. Rev. 44, 39–79.

Hole, M.J., Saunders, A.D., Marriner, G.F., Tarney, J., 1984. Subduction of pelagic sediments: implications for the origin of Ce-anomalous basalts from the Mariana islands. J. Geol. Soc. Lond. 141, 453–472.

Hollings, P., Wyman, D., Kerrich, R., 1999. Komatiite–basalt–rhyolite volcanic associations in Northern Superior Province greenstone belts: significance of plume–arc interaction in the generation of the proto continental Superior Province. Lithos 46, 137–161.

Holloway, J.R., Burnham, C.W., 1972. Melting relations of basalt with equilibrium water pressure less than total pressure. J. Petrol. 13, 1–29.

Horstwood, M.S.A., Nesbitt, R.W., Noble, S.R., Wilson, J.F., 1999. U–Pb zircon evidence for an extensive early Archean craton in Zimbabwe: a reassessment of the timing of craton formation, stabilization and growth. Geology 27, 707–710.

Houseman, G.A., McKenzie, D.P., Molnar, P., 1981. Convective instability of a thickened boundary layer and its relevance for the thermal evolution of continental convergence belts. J. Geophys. Res. 86, 6115–6132.

Hunter, M.A., Bickle, M.J., Nisbet, E.G., Martin, A., Chapman, H.J., 1998. Continental extensional setting for the Archean Belingwe greenstone belt, Zimbabwe. Geology 26, 883–886.

Hyndman, D.W., Foster, D.A., 1988. The role of tonalites and mafic dykes in the generation of Idaho batholith. J. Petrol. 25, 894–929.

James, D.E., Fouch, M.J., VanDecar, J.C., van der Lee, S., the Kaapvaal Seismic Group, 2001. Tectospheric structure beneath southern Africa. Geophys. Res. Lett. 28, 2485–2488.

Jelsma, H.A., Dirks, P.H.G.M., 2000. Tectonic evolution of a greenstone sequence in northern Zimbabwe: sequential early stacking and pluton diapirism. Tectonics 19, 135–152.

Jelsma, H.A., Vinyu, M.L., Valbracht, P.J., Davies, G.R., Wijbrans, J.R., Verdurmen, E.A.T., 1996. Constraints on Archaean crustal evolution of the Zimbabwe craton: a U–Pb zircon, Sm–Nd and Pb–Pb whole-rock isotope study. Contrib. Mineral. Petrol. 124, 55–70.

Jelsma, H.A., Becker, J.K., Siegesmund, S., 2001. Geochemical characteristics and tectonomagmatic evolution of the Chinamora batholith, Zimbabwe. Z. Dtsch. Geol. Ges. 152, 199–225.

Jenner, G.A., Longerich, H.P., Jackson, S.E., Fryer, B.J., 1990. ICP-MS—a powerful tool for high-precision trace-element analysis in Earth Sciences: evidence from analysis of selected U.S.G.S. reference samples. Chem. Geol. 83, 133–148.

Kamber, B.S., Biino, G.G., 1995. The evolution of high T–low P granulites in the Northern Marginal Zone sensu stricto, Limpopo belt, Zimbabwe—the case for petrography. Schweiz. Mineral. Petrogr. Mitt. 75, 427–454.

Kamber, B.S., Collerson, K.D., 2000. Role of "hidden" deeply subducted slabs in mantle depletion. Chem. Geol. 166, 241–254.

Kamber, B.S., Biino, G.G., Wijbrans, J.R., Davies, G.R., Villa, I.M., 1996. Archaean granulites of the Limpopo belt, Zimbabwe: one slow exhumation or two rapid events? Tectonics 15, 1414–1430.

Kampunzu, A.B., Akanyang, P., Mapeo, R.B.M., Modie, B.N., Wendorff, M., 1998. Geochemistry and tectonic significance of Mesoproterozoic Kgwebe metavolcanic rocks in northwest Botswana: implications for the evolution of the Kibaran Namaqua-Natal belt. Geol. Mag. 133, 669–683.

Kampunzu, A.B., Ramakgala, M., Paya, B.K., McCourt, S., Mitchell, A., Hoffmann, D., Witley, J., 2002. Archaean podiform chromitite from the Phikwe Ni–Cu sulphide deposit (Limpopo belt, NE Botswana): chrome spinel and host-rock chemistry, implications for geotectonic setting. Lithos (this volume, submitted).

Kapenda, D., Kampunzu, A.B., Cabanis, B., Namegabe, M., Tshimanga, K., 1998. Petrology and geochemistry of post-kinematic mafic rocks from the Paleoproterozoic Ubendian belt, NE Katanga (Democratic Republic of Congo). Geol. Rundsch. 87, 345–362.

Kay, S.M., Abbruzzi, J.M., 1996. Magmatic evidence for Neogene lithospheric evolution of the central Andean "flat-slab" between 30°S and 32°S. Tectonophysics 259, 15–28.

Kelemen, P.B., 1995. Genesis of the high Mg andesites and the continental crust. Contrib. Mineral. Petrol. 120, 1–19.

Kelemen, P.B., Shimizu, N., Dunn, T., 1993. Relative depletion of niobium in some arc magmas and the continental crust: partitioning of K, Nb, La and Ce during melt/ rock reaction in the upper mantle. Earth Planet. Sci. Lett. 120, 111–134.

Kepezhinskas, P.K., Defant, M.J., Drummond, M.S., 1996. Progressive enrichment of island arc mantle by melt–peridotite inter-

action inferred from Kamchatka xenoliths. Geochim. Cosmochim. Acta 60, 1217–1229.
Keppler, H., 1996. Constraints from partitioning experiments on the composition of subduction-zone fluids. Nature 380, 237–240.
Key, R.M., Litherland, M., Hepworth, J.V., 1976. The evolution of the Archaean crust of northeast Botswana. Precambrian Res. 3, 375–413.
Kröner, A., Jaeckel, P., Brandle, G., Nemchin, A.A., Pidgeon, R.T., 1999. Single zircon ages for granitoid gneisses in the Central Zone of the Limpopo belt, southern Africa and geodynamic significance. Precambrian Res. 93, 299–337.
Kusky, T.M., 1998. Tectonic setting and terrane accretion of the Archean craton. Geology 26, 163–166.
Kusky, T.M., Kidd, W.S.F., 1992. Remnants of an Archaean oceanic plateau, Belingwe greenstone belt, Zimbabwe. Geology 20, 43–46.
Luais, B., Hawkesworth, C.J., 1994. The generation of continental crust: an integrated study of crust-forming processes in the Archaean of Zimbabwe. J. Petrol. 35, 43–93.
Majaule, T., Davis, D.W., 1998. U–Pb zircon dating and geochemistry of granitoids in the Mosetse area, NE Botswana, and tectonic implications. Geol. Surv. Botswana, 50th. Anniversary Internat. Conf. Abstr. Vol, pp. 46–48.
Majaule, T., Hall, P., Hughes, D., 1997. Geochemistry of mafic and ultramafic igneous rocks of the Matsitama supracrustal belt, northeastern Botswana—provenance implications. S. Afr. J. Geol. 100, 169–179.
Martin, H., 1993. The mechanism of petrogenesis of the Archean continental crust—comparison with modern processes. Lithos 30, 373–388.
Martin, H., 1994. The Archaean grey gneisses and the genesis of the continental crust. In: Condie, K.C. (Ed.), The Archaean Crustal Evolution. Elsevier, Amsterdam, pp. 205–259.
McCourt, S., Wilson, J.F., 1992. Late Archaean and early Proterozoic tectonics, Limpopo and Zimbabwe. In: Glover, J.E., Ho, S.E. (Eds.), The Archaean: Terrains, Processes and Metallogeny. Proceedings Third Internat. Archaean Symposium, Perth, University Western Australia Public, Nr. 22, 237–246.
McCulloh, M.T., 1993. The role of subducted slabs in an evolving earth. Earth Planet. Sci. Lett. 115, 89–100.
Mkweli, S., Kamber, B., Berger, M., 1995. Westward continuation of the Craton–Limpopo belt tectonic break in Zimbabwe and new age constraints on the timing of the thrusting. J. Geol. Soc. Lond. 152, 77–83.
Nägler, Th.F., Kramers, J.D., Kamber, B.S., Frei, R., Predergast, M.D.A., 1997. Growth of subcontinental lithospheric mantle beneath Zimbabwe started at or before 3.8 Ga: Re–Os study on chromites. Geology 25, 983–986.
Nguuri, T.K., Gore, J., James, D.E., Wright, C., Zengeni, T.D., Gwavava, O., Webb, S.J., Snoke, J.A., the Kaapvaal Seismic Group, 2001. Crustal structure beneath southern Africa and its implications for the formation and evolution of the Kaapvaal and Zimbabwe cratons. Geophys. Res. Lett. 28, 2501–2504.
Nisbet, E.G., Wilson, J.F., Bickle, M.J., 1981. The evolution of the Rhodesian craton and adjacent Archaean terrain: tectonic models. In: Kröner, A. (Ed.), Precambrian Plate Tectonics. Elsevier, Amsterdam, pp. 161–183.
Parman, S.W., Dann, J.C., Grove, T.L., de Wit, M.J., 1997. Emplacement conditions of komatiites magmas from the 3.49 Ga Komati Formation, Barberton Greenstone Belt, South Africa. Earth Planet. Sci. Lett. 150, 303–323.
Patiño Douce, A.E., Beard, J.S., 1995. Dehydration melting of biotite gneiss and quartz amphibolite from 3 to 15 kbar. J. Petrol. 36, 707–738.
Peacock, S.M., Rushmer, T., Thompson, A.B., 1994. Partial melting of subducting oceanic crust. Earth Planet. Sci. Lett. 121, 224–244.
Pearce, J.A., 1982. Trace element characteristics of lavas from destructive plate boundaries. In: Thorpe, R.S. (Ed.), Andesites. Wiley, New York, pp. 525–548.
Pearce, J.A., Harris, N.B.W., Tindle, A.G., 1984. Trace element discrimination diagrams for the tectonic interpretation of granitic rocks. J. Petrol. 25, 956–983.
Petford, N., Atherton, M., 1996. Na-rich partial melts from newly underplated basaltic crust: the Cordillera Blanca Batholith, Peru. J. Petrol. 37, 1491–1521.
Pitcher, W.S., 1993. The Nature and Origin of Granites. Blackie, Glasgow. 316 pp.
Plank, T., Langmuir, C.H., 1993. Tracing trace elements from sediment input to volcanic output at subduction zones. Nature 362, 739–742.
Plank, T., Langmuir, C.H., 1998. The chemical composition of subducting sediment and its consequences for the crust and mantle. Chem. Geol. 145, 325–394.
Pubellier, M., Cobbold, P., 1996. Analogue models for the transpressional docking of volcanic arcs in the western Pacific. Tectonophysics 253, 33–52.
Ranganai, R.T., Kampunzu, A.B., Atekwana, E.A., Paya, B.K., King, J.G., Koosimile, D.I., Stettler, E.H., 2002. Gravity evidence for a larger Limpopo belt in southern Africa and geodynamic implications. Geophys. J. Int. 149, F9–F14.
Rapp, 1997. Heterogeneous source for Archaean granitoids: experimental and geochemical evidence. In: de Wit, M.J., Ashwal, L.D. (Eds.), 1997. Greenstone Belts. Clarendon Press, New York, pp. 267–279.
Rapp, R.P., Watson, E.B., Miller, C.F., 1991. Partial melting of amphibolite/eclogite and the origin of Archean trondhjemites and tonalites. Precambrian Res. 94, 4619–4633.
Rapp, R.P., Shimizu, N., Norman, M.D., Applegate, G.S., 1999. Reaction between slab melts and peridotite in the mantle wedge: experimental constraints at 3.8 GPa. Chem. Geol. 160, 335–356.
Roberts, M.P., Clemens, J.D., 1993. Origin of high-potassium, calc-alkaline, I-type granitoids. Geology 21, 825–828.
Rollinson, H.R., 1993. A terrane interpretation of the Archaean Limpopo belt. Geol. Mag. 130, 755–765.
Rushmer, T., 1991. Partial melting of two amphibolites: contrasting experimental results under fluid-absent conditions. Contrib. Mineral. Petrol. 107, 41–59.
Ryan, J.G., Morris, J., Tera, F., Leeman, W.P., Tsvetkov, A., 1995. Cross-arc geochemical variations in the Kurile arc as a function of slab depth. Science 270, 625–627.
Sajona, F.G., Maury, R.C., Bellon, H., Cotten, J., Defant, M.J., Pubellier, M., Rangin, C., 1993. Initiation of subduction and

the generation of slab melts in western and eastern Mindanao, Phillippines. Geology 21, 1007–1010.

Sajona, F.G., Maury, R.C., Pubellier, M., Leterrier, J., Bellon, H., Cotton, J., 2000. Magmatic source enrichment by slab-derived melts in a young post-collision setting, central Mindanao (Philippines). Lithos 54, 173–206.

Schiano, P., Clochiatti, R., Shimizu, N., Maury, R.C., Jochum, K.P., Hofmann, A.W., 1995. Hydrous silica-rich melts in the sub-arc mantle and their relationship with erupted arc lavas. Nature 377, 595–600.

Sen, C., Dunn, T., 1994. Dehydration melting of a basaltic composition amphibolite at 1.5 and 2.0 GPa: implications for the origin of adakites. Contrib. Mineral. Petrol. 117, 394–409.

Sen, C., Dunn, T., 1995. Experimental modal metasomatism of a spinel lherzolite and the production of amphibole bearing peridotite. Contrib. Mineral. Petrol. 119, 394–409.

Shimoda, G., Tatsumi, Y., Nohda, S., Ishizaka, K., Jahn, B.M., 1998. Setouchi high-Mg andesites revisited: geochemical evidence for melting of subducting sediments. Earth Planet. Sci. Lett. 160, 479–492.

Shirey, S.B., Hanson, G.N., 1984. Mantle-derived Archean monzodiorites and trachyandesites. Nature 310, 222–224.

Spencer, J.E., 1994. A numerical assessment of slab strength during high- and low-angle subduction and implications for Laramide orogenesis. J. Geophys. Res. 99, 9227–9236.

Stern, R.A., Hanson, G.N., 1991. Archean high-Mg granodiorite: a derivative of light rare earth element-enriched monzodiorite of mantle origin. J. Petrol. 32, 201–238.

Stern, R.A., Hanson, G.N., Shirey, S.B., 1989. Petrogenesis of mantle-derived, LILE-enriched Archean monzodiorite and trachyandesites (Sanukitoids) in Southwestern Superior Province. Can. J. Earth Sci. 26, 1688–1712.

Stevenson, R., Henry, P., Gariepy, C., 1999. Assimilation-fractional crystallization origin of Archean Sanukitoid suites: Western Superior Province, Canada. Precambrian Res. 96, 83–99.

Stolper, E., Newman, S., 1994. The role of water in the petrogenesis of Mariana trough magmas. Earth Planet. Sci. Lett. 121, 293–325.

Sun, S.S., McDonough, W.F., 1989. Chemical and isotopic systematics of oceanic basalts: implications for mantle composition and processes. In: Saunders, A.D., Norry, M.J. (Eds.), Magmatism in the Ocean Basins. Geol. Soc. London Spec. Publ., vol. 42, pp. 313–345.

Tatsumi, Y., Ishizaka, K., 1982. Origin of high-magnesian andesites in the Setouchi volcanic belt, southwest Japan: I. Petrographical and chemical characteristics. Earth Planet. Sci. Lett. 60, 293–304.

Tatsumi, Y., Kogiso, T., 1997. Trace element transport during dehydration processes in the subducted oceanic crust: 2. Origin of chemical and physical characteristics in arc magmatism. Earth Planet. Sci. Lett. 148, 207–221.

Tchameni, R., Mezger, K., Nsifa, N.E., Pouclet, A., 2000. Neoarchaean crustal evolution of the Congo craton: evidence from K-rich granitoids of the Ntem Complex, southern Cameroon. J. Afr. Earth Sci. 30, 133–147.

Tepper, J.H., Nelson, B.K., Bergantz, G.W., Irving, A.J., 1993. Petrology of the Chilliwack batholith, North Cascades, Washington: generation of calc-alkaline granitoids by melting of mafic lower crust with variable water fugacity. Contrib. Mineral. Petrol. 113, 333–351.

Thorpe, R.S. (Ed.), 1982. Andesites: Orogenic Andesites and Related Rocks. Wiley, Chichester. 724 pp.

Tombale, A.R., 1992. The geology, geochemistry and metallogeny of the Tati Greenstone belt, northeastern Botswana. PhD Thesis, Memorial University of Newfoundland, Canada. 383 pp.

Treloar, P.J., Blenkinsop, T.G., 1995. Archaean deformation patterns in Zimbabwe: true indicators of Tibetan-style crustal extrusion or not? Geol. Soc. London Spec. Publ. 95, 87–108.

Treloar, P.J., Coward, M.P., Harris, N.B.W., 1992. Himalayan–Tibetan analogies for the evolution of the Zimbabwe craton and Limpopo belt. Precambrian Res. 55, 571–587.

Vidal, P., Dupuy, C., Maury, R., Richard, M., 1989. Mantle metasomatism above subduction zones: trace element and radiogenic isotope in xenoliths from Batuan island (Philippines). Geology 17, 1115–1118.

Vlaar, N.J., 1983. Thermal anomalies and magmatism due to lithospheric doubling and shifting. Earth Planet. Sci. Lett. 65, 322–330.

Walker, J.A., Patino, L.C., Cameron, B.I., Carr, M.J., 2000. Petrogenetic insights provided by compositional transects across the Central American arc: southeastern Guatemala and Honduras. J. Geophys. Res. 105 (B8), 18949–18963.

Wickham, S.M., 1987. The generation and emplacement of granitic magmas. J. Geol. Soc. Lond. 144, 281–297.

Wilson, J.F., Nesbitt, R.W., Fanning, C.M., 1995. Zircon geochronology of Archaean felsic sequences in the Zimbabwe craton: a revision of greenstone stratigraphy and a model for crustal growth. In: Coward, M.P., Ries, A.C. (Eds.), Early Precambrian Processes. Geol. Soc. London Spec. Publ., vol. 95, pp. 109–126.

Wolf, M.B., Wyllie, P.J., 1994. Dehydration melting of solid amphibolite at 10 kbar: the effects of temperature and time. Contrib. Mineral. Petrol. 115, 369–383.

Wood, D.A., Joron, J.L., Treuil, M., 1979. A re-appraisal of the use of trace elements to classify and discriminate between magma series erupted in different tectonic settings. Earth Planet. Sci. Lett. 45, 326–336.

Wyllie, P.J., Wolf, M.B., van der Laan, S.R., 1997. Conditions for formation of tonalites and trondhjemites: magmatic sources and products. In: de Wit, M.J., Ashwal, L.D. (Eds.), Greenstone Belts. Clarendon Press, New York, pp. 256–266.

Yogodzinski, G.M., Kay, R.W., Volynets, O.N., Koloskov, A.V., Kay, S.M., 1995. Magnesian andesite in the western Aleutian Komandorsky region: implications for slab melting and processes in the mantle wedge. Geol. Soc. Am. Bull. 107, 505–519.

You, C.F., Castillo, P.R., Gieskes, J.M., Chan, L.H., Spivack, A.J., 1996. Trace element behavior in hydrothermal experiments: implications for fluid processes at shallow depths in subduction zones. Earth Planet. Sci. Lett. 140, 41–52.